



Dual CD4-based CAR T cells with distinct costimulatory domains mitigate HIV pathogenesis in vivo

Colby R. Maldini^{1,6}, Daniel T. Claiborne^{2,6}, Ken Okawa², Tao Chen², Derrick L. Dopkin³, Xiaochuan Shan³, Karen A. Power², Radiana T. Trifonova², Katharine Krupp², Meredith Phelps², Vladimir D. Vrbanc^{2,4}, Serah Tanno^{2,4}, Timothy Bateson², George J. Leslie⁵, James A. Hoxie⁵, Christian L. Boutwell², James L. Riley^{1,7}✉ and Todd M. Allen^{1,7}✉

An effective strategy to cure HIV will likely require a potent and sustained antiviral T cell response. Here we explored the utility of chimeric antigen receptor (CAR) T cells, expressing the CD4 ectodomain to confer specificity for the HIV envelope, to mitigate HIV-induced pathogenesis in bone marrow, liver, thymus (BLT) humanized mice. CAR T cells expressing the 4-1BB/CD3- ζ endodomain were insufficient to prevent viral rebound and CD4⁺ T cell loss after the discontinuation of antiretroviral therapy. Through iterative improvements to the CAR T cell product, we developed Dual-CAR T cells that simultaneously expressed both 4-1BB/CD3- ζ and CD28/CD3- ζ endodomains. Dual-CAR T cells exhibited expansion kinetics that exceeded 4-1BB-, CD28- and third-generation costimulated CAR T cells, elicited effector functions equivalent to CD28-costimulated CAR T cells and prevented HIV-induced CD4⁺ T cell loss despite persistent viremia. Moreover, when Dual-CAR T cells were protected from HIV infection through expression of the C34-CXCR4 fusion inhibitor, these cells significantly reduced acute-phase viremia, as well as accelerated HIV suppression in the presence of antiretroviral therapy and reduced tissue viral burden. Collectively, these studies demonstrate the enhanced therapeutic potency of a novel Dual-CAR T cell product with the potential to effectively treat HIV infection.

CAR T cell immunotherapies, in which engineered T cells are infused into patients, have induced durable remissions for treatment-refractory malignancies¹. Although a potent and sustained T cell response of the kind that CAR T cells can afford is likely to be essential for the development of an effective HIV cure², a successful CAR T cell therapy for HIV infection has remained elusive. CARs redirect T cell specificity by expressing an extracellular antigen recognition domain linked to an intracellular T cell costimulatory domain and the CD3- ζ chain^{3,4}. The costimulatory domains for second-generation CARs are derived from the intracellular signaling domains of either CD28 or 4-1BB, which is one of the key differences between the two Food and Drug Administration-approved CD19-targeting CAR T cell therapies^{5,6}. Preclinical cancer models demonstrate that CD28-costimulated CAR T cells exhibit profound effector function resulting in rapid tumor clearance, but have limited persistence in vivo^{7,8}. In contrast, 4-1BB-costimulated CAR T cells have a slower antitumor response but sustained proliferation and survival^{9–12}. The distinct signaling pathways used by CD28 and 4-1BB cause distinct metabolic, phenotypic and functional T cell profiles that can elicit optimal CAR T cell activity for specific diseases^{13–17}, and there is great interest in tuning costimulatory signals to optimize CAR T cell function^{18,19}.

The earliest clinical trials of CAR T cell therapy used first-generation, CD4-based CARs targeting the HIV Envelope

glycoprotein via surface expression of the CD4 ectodomain and proved ineffective for treatment of either chronic or antiretroviral therapy (ART)-suppressed infection^{20–22}. However, subsequent significant improvements in CAR technology by the cancer immunotherapy field have renewed interest in applying these advances to HIV treatment^{23–29}. The continued investigation of the mechanistic underpinnings of successful and failed CAR T cell therapy, particularly in a model system that recapitulates HIV pathogenesis, will be critical for the development of a CAR T therapy for HIV cure initiatives.

Here we used the BLT humanized mouse model of HIV infection to iteratively test CD28 and 4-1BB costimulation in the context of optimizing HIV-specific CAR T cell therapy. We leveraged the BLT mouse model's ability to support HIV infection, including high viral loads, rapid human CD4⁺ T cell depletion and ultimately T cell exhaustion^{30–33}, to make stepwise improvements to the CAR T cell product (TCP). This effort culminated in the development of HIV-resistant (C34-CXCR4⁺), Dual-CAR T cells that express two CD4-based CARs independently encoding the CD28/CD3- ζ and 4-1BB/CD3- ζ endodomains. Collectively, these data provide important insight regarding the development of an engineered T cell-based therapy of HIV infection and highlight the novel function of a Dual-CAR TCP that mitigates HIV-induced disease.

¹Department of Microbiology, Center for Cellular Immunotherapies, Perelman School of Medicine, University of Pennsylvania, Philadelphia, PA, USA. ²Ragon Institute of MGH, MIT and Harvard, Cambridge, MA, USA. ³Department of Pathology & Laboratory Medicine, Perelman School of Medicine, University of Pennsylvania, Philadelphia, PA, USA. ⁴Human Immune System Mouse Program, Massachusetts General Hospital, Boston, MA, USA. ⁵Department of Medicine, Perelman School of Medicine, University of Pennsylvania, Philadelphia, PA, USA. ⁶These authors contributed equally: Colby R. Maldini, Daniel T. Claiborne. ⁷These authors jointly supervised this work: James L. Riley, Todd M. Allen. ✉e-mail: rileyj@upenn.edu; tallen2@mgh.harvard.edu

Results

BLT mouse-derived CAR T cells are multifunctional and suppress HIV replication in vitro. To determine whether T cells isolated from BLT mice generate potent CAR TCPs, we manufactured HIV-specific (CD4-based) CAR T cells expressing the CD3- ζ endodomain (CAR. ζ) from BLT mouse tissues and adult human peripheral blood mononuclear cells (PBMCs) (Supplementary Fig. 1a). BLT mouse- and human-derived CAR. ζ T cells exhibited comparable in vitro expansion kinetics and CAR surface expression levels (Supplementary Fig. 1b and Fig. 1a). Antigen-specific stimulation with K562 cells expressing HIV_{YU2} Envelope (K.Env) induced similar cytokine expression and polyfunctionality profiles between the CAR T cell sources (Fig. 1b,c and Supplementary Fig. 1c–e). Furthermore, CAR. ζ T cells from both donors suppressed viral outgrowth down to a 1:50 effector/target ratio in vitro (Fig. 1d,e), and induced similar levels of cleaved caspase-3 in HIV-infected CD4⁺ T cells (Supplementary Fig. 1f and Fig. 1f,g). The induction of caspase-3 combined with the coregulation of granzyme B and perforin by CAR. ζ T cells (Supplementary Fig. 1g,h) indicates that elimination of virus-infected cells likely occurred via granule-mediated cytotoxicity. In total, the in vitro functional profile of BLT mouse-derived CAR. ζ T cells was indistinguishable from that of human-derived CAR. ζ T cells, demonstrating that highly functional CAR T cells can be manufactured from BLT mice.

Costimulation modulates CAR T cell persistence and function in vivo. To identify a CAR TCP capable of long-term persistence against HIV, we compared the contribution of costimulatory domains with in vivo engraftment of T cells by creating an infusion product comprising equal frequencies of HIV-specific CAR.CD3- ζ (CAR. ζ), 4-1BB/CD3- ζ (CAR.BB ζ) and CD28/CD3- ζ (CAR.28 ζ) T cells, each of which was linked to a distinct fluorescent protein (Fig. 2a). After infusion, CAR.BB ζ T cells exhibited significantly greater survival in the absence of HIV antigen (Fig. 2b–d), and constituted approximately 80% of total CAR T cells in tissues (Fig. 2e). Consistent with reports from the cancer field^{9–12}, CAR.BB ζ T cells also demonstrated superior in vivo antigen-driven proliferation upon infusion of K.Env cells (Fig. 2f). In contrast, CAR.28 ζ T cells only exhibited a transient expansion followed by a progressive decline, and CAR. ζ T cells steadily declined demonstrating no evidence of expansion. Notably, however, CAR.28 ζ T cells exhibited greater effector functions when stimulated ex vivo with K.Env cells, upregulating more MIP-1 β , TNF and IL-2, and coexpressing greater levels of granzyme B and perforin than CAR.BB ζ T cells from the same mice (Fig. 2g,h and Extended Data Fig. 1). Finally, we confirmed the in vivo cytotoxic potential of BLT mouse-derived CAR T cells by infusing CD19-specific CAR.BB ζ T cells into recipient mice. We observed rapid and profound B cell aplasia in the blood (Fig. 2i), as well as in the spleen, lung, liver and bone marrow, consistent with a sustained cytotoxic CAR T cell response (Fig. 2j,k). Together, these data demonstrate the suitability of BLT mice for studying in vivo CAR T cell function, and the degree to which costimulation can modulate CAR T cell activity.

CAR.BB ζ T cells fail to control HIV rebound upon ART discontinuation. After determining that the 4-1BB/CD3- ζ endodomain confers superior in vivo antigen-driven CAR T cell expansion and persistence, we sought to test the therapeutic potential of CAR.BB ζ T cells in the context of ART-suppressed HIV infection. To do so, we infected BLT mice with CCR5-tropic HIV_{JRC5F} and after 3 weeks initiated ART. At 2 weeks later, ART-suppressed mice were allocated into groups that received an infusion of either CAR.BB ζ T cells (Group 1 (G1) and Group 3 (G3)), or inactive control CAR.BB $\Delta\zeta$ T cells (Group 2 (G2) and Group 4 (G4)), which express a truncated CD3- ζ chain. In G1 and G2, ART was ceased immediately after infusion, whereas in G3 and G4 ART was continued

for an additional 3 weeks to test whether the timing of ART interruption impacted the efficacy of CAR T cell therapy. In all groups, HIV rebounded by 2 weeks after treatment interruption, regardless of timing, and there were no observable differences in the kinetics or magnitude of viremia in CAR.BB ζ -treated mice compared with matched control mice (Fig. 3a). Moreover, CAR.BB ζ T cell therapy did not prevent memory CD4⁺ T cell loss in peripheral blood or tissues (Fig. 3b,c and Supplementary Fig. 2), which in BLT mice represents the CD4⁺ T cell subset preferentially infected and depleted by HIV due to high levels of CCR5 expression (Supplementary Fig. 3). Together, these data indicate that CAR.BB ζ T cell therapy did not impact HIV progression.

CAR.BB ζ T cells display features of T cell exhaustion during uncontrolled HIV replication. Despite the lack of efficacy following ART discontinuation, we observed profound CAR.BB ζ T cell expansion during viral recrudescence with a median 75-fold increase in the blood (Fig. 3d,e). As expected, the control T cells did not expand in response to viral rebound (Fig. 3d,e), and the CAR.BB ζ T cells were substantially more abundant throughout the body 12 weeks after infusion (Fig. 3f). These findings suggested that the inability of CAR.BB ζ T cells to control viremia and HIV pathogenesis was not the result of poor proliferation, poor persistence or lack of migration to relevant anatomical compartments of virus replication^{34–36}.

The proliferation of CAR.BB ζ T cells was associated with upregulation of inhibitory receptors including PD-1, TIGIT and 2B4, which increased over time (Fig. 3g and Extended Data Fig. 2a–d). Importantly, these inhibitory receptors were not expressed to the same extent on endogenous CAR⁺ T cells within the same mice, suggesting a CAR T cell-specific effect rather than generalized activation from inflammation or viral load (Extended Data Fig. 2e,f). Notably, elevated inhibitory receptor expression on CAR.BB ζ T cells from chronically infected mice was associated with the expression of TOX (Fig. 3h,i), a transcription factor that regulates the T cell exhaustion program^{37–41}. Further supporting the gradual emergence of a dysfunctional CAR T cell phenotype, T-bet expression in CAR.BB ζ T cells waned as HIV infection progressed, culminating in a population of Eomes^{hi}T-bet^{dim} CAR T cells that were enriched in TOX expression and accumulated in tissues with higher viral burden (Fig. 3j,k and Extended Data Fig. 3). In addition, expression of multiple inhibitory receptors on CAR.BB ζ T cells from chronic infection was linked to a transitional memory state that also displayed an Eomes^{hi}T-bet^{dim} phenotype (Fig. 3l), all of which is congruent with earlier studies identifying dysfunctional HIV-specific CD8⁺ T cells within this compartment in chronic human HIV infection^{42,43}.

Finally, we compared the ex vivo functions of CAR.BB ζ T cells isolated during chronic infection with the preinfusion CAR TCP. Although the CD8⁺ CAR.BB ζ T cells from chronic infection retained the ability to upregulate MIP-1 β and granzyme B, and degranulate based on CD107a expression, the degree of β -chemokine production and cytotoxic potential was attenuated (Supplementary Fig. 4). Taken together, these data indicate that CAR.BB ζ T cells recognize HIV-infected cells, rapidly expand and upregulate markers of cellular activation, but that uncontrolled virus replication ultimately drives an exhaustion program that may diminish T cell function and subvert efficacy.

Augmented HIV-specific CAR TCP reduces CD4⁺ T cell loss during acute infection. We hypothesized that combining the superior in vivo expansion and persistence of CAR.BB ζ T cells with enhanced effector function could provide the necessary improvement to control HIV replication. To this end, we cotransduced CAR.BB ζ T cells with the CD4-based, CD28-costimulated CAR that exhibited notable effector function (Extended Data Fig. 1) to create a novel Dual-CAR TCP. Due to cotransduction

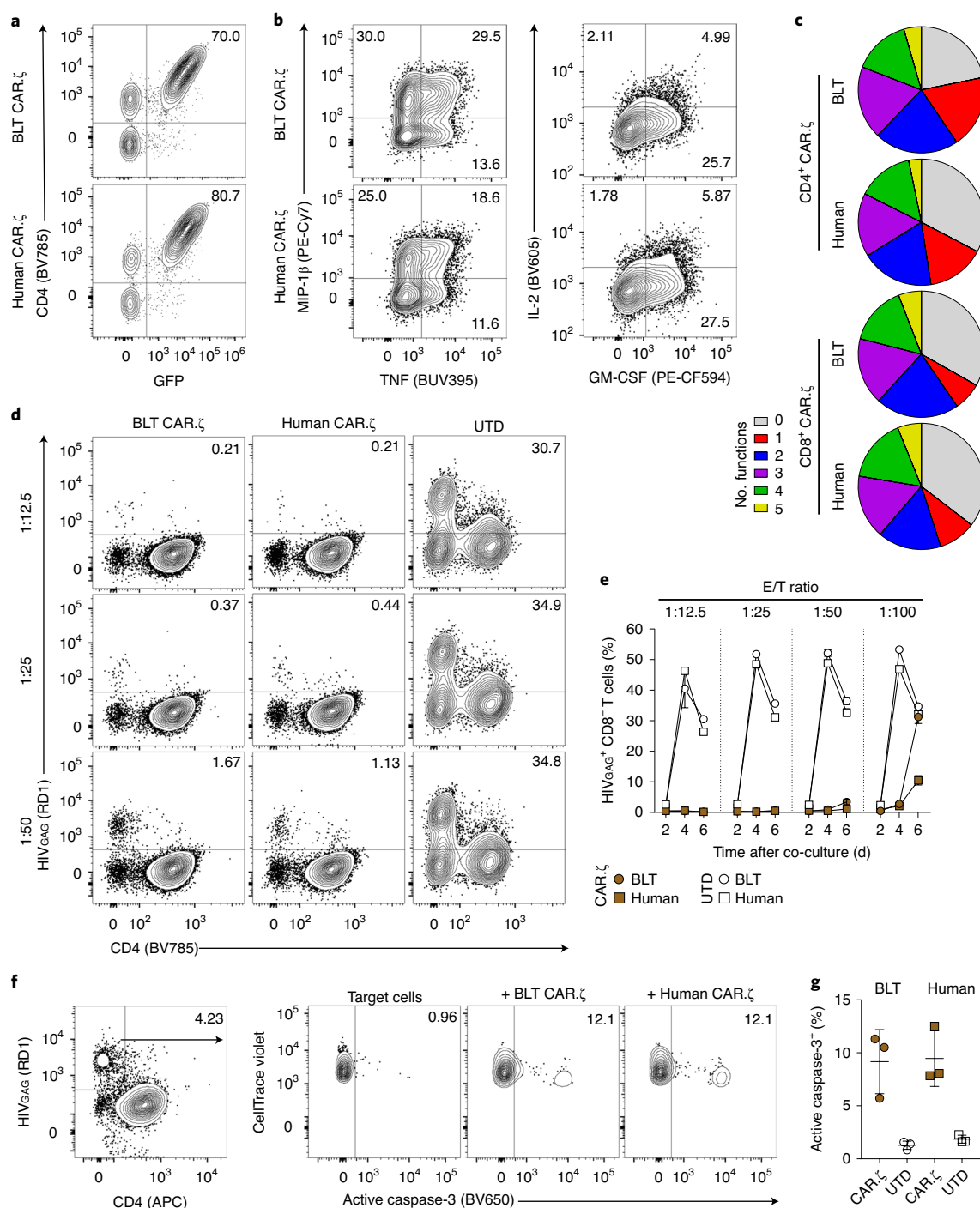


Fig. 1 | BLT mouse-derived HIV-specific CAR T cells are functionally indistinguishable from human-derived CAR T cells in vitro. α CD3/CD28 Dynabeads were used to activate purified human T cells from a BLT mouse and healthy human donor, and then cells were transduced with the CD4-based CAR.ζ construct coexpressing GFP. **a**, FACS plots identify CAR.ζ T cells from each T cell source as GFP⁺ and CD4⁺. **b**, Following 10 d of culture, CD8⁺ CAR.ζ T cells were mixed with HIV_{YU2} Envelope⁺ K562 cells (K.Env) and upregulation of human cytokines was measured. **c**, Polyfunctionality profiles for combinatorial subsets of CD4⁺ and CD8⁺ CAR.ζ T cells producing 0 to 5 of the human cytokines GM-CSF, IFN-γ, IL-2, MIP-1β and TNF. Average of three unique donors per T cell source. **d**, HIV suppression assay as described in the Methods. **e**, FACS plots indicating the frequency of HIV-infected cells 6 d after coculturing with BLT mouse- or human-derived CAR.ζ T cells at denoted E/T ratios. **f**, Summary of frequency of HIV-infected cells (live CAR⁻ CD8⁻ cells) at 2, 4 and 6 d after coculture with BLT mouse- or human-derived CAR.ζ and untransduced (UTD) T cells at indicated E/T ratios. **g**, HIV elimination assay as described in the Methods. FACS plots (**f**) and summarized data (**g**) for frequency of active caspase-3 within HIV-infected cells (live CTV⁺ HIV_{GAG}⁺ cells) 24 h after coculture with BLT mouse- or human-derived CAR.ζ and UTD T cells at 1:1 E/T ratio. Each symbol represents the average of technical duplicates per donor ($n = 3$ biologically independent donors). **e**, **g**, Symbols and lines reflect mean and error bars indicate \pm s.e.m. RD1 is another name for phycoerythrin (PE).

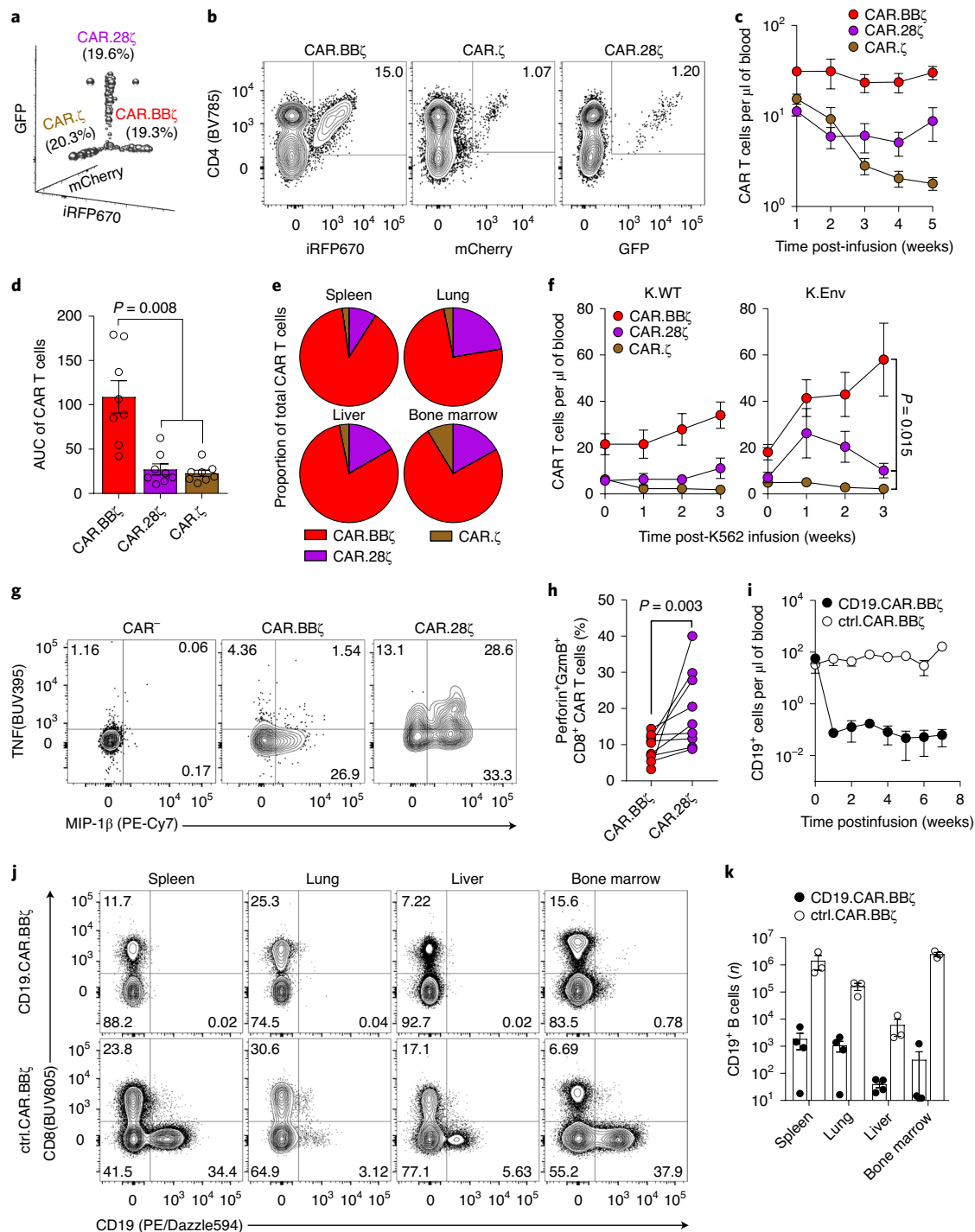


Fig. 2 | CAR T cells expressing the 4-1BB costimulatory domain exhibit a proliferative advantage and induce B cell aplasia in vivo. **a–e**, BLT mouse-derived T cells were transduced with mCherry.T2A.CAR. ζ , iRFP670.T2A.CAR.BB ζ or GFP.T2A.CAR.28 ζ . In total, 5×10^6 CAR-transduced T cells of each type were mixed before infusion into syngeneic mice ($n = 8$). **a**, Frequency of each CAR T cell type within the preinfusion TCP. **b**, Frequency of peripheral CAR T cells within the same mouse at 5 weeks postinfusion. **c, d**, Peripheral concentration (**c**) and cumulative persistence (**d**) of each CAR T cell type over 5 weeks of engraftment. **e**, Relative tissue frequency of each CAR T cell type at 7 weeks postinfusion. **f**, In a separate study, 2 weeks after infusion of the CAR T cell mixture described in **a**, BLT mice received 10^7 irradiated K.WT ($n = 8$) or HIV $_{\text{Env}}$ (K.Env; $n = 8$) K562 cells. Peripheral concentration of each CAR T cell type following K.WT or K.Env infusion. **g**, FACS plots indicating frequency of MIP-1 β $^{+}$ and TNF $^{+}$ CAR.BB ζ and CAR.28 ζ T cells within the same mouse after ex vivo stimulation. CAR. ζ T cells were too infrequent for analysis. **h**, Frequency of granzyme B $^{+}$ perforin $^{+}$ CD8 $^{+}$ CAR T cells within the same mice ex vivo. **i–k**, Mice were infused with 5×10^6 CD19-specific CAR.BB ζ ($n = 4$) or control CD4-based CAR.BB ζ T cells ($n = 3$). **i**, Concentration of peripheral CD19 $^{+}$ cells following infusion. **j, k**, FACS plots showing frequency of CD19 $^{+}$ cells (**j**), and number of CD19 $^{+}$ cells (**k**) in tissues at 7 weeks postinfusion. For all data, symbols and bars reflect mean and error bars show \pm s.e.m., except **d** and **k** where symbols represent individual mice. **d**, Friedman's test with Dunn's multiple corrections test. **f, h**, Two-sided Wilcoxon matched-pairs signed rank test was performed to calculate significance. Sample sizes for all mouse groups indicate biologically independent animals. AUC, area under the curve; ctrl, control.

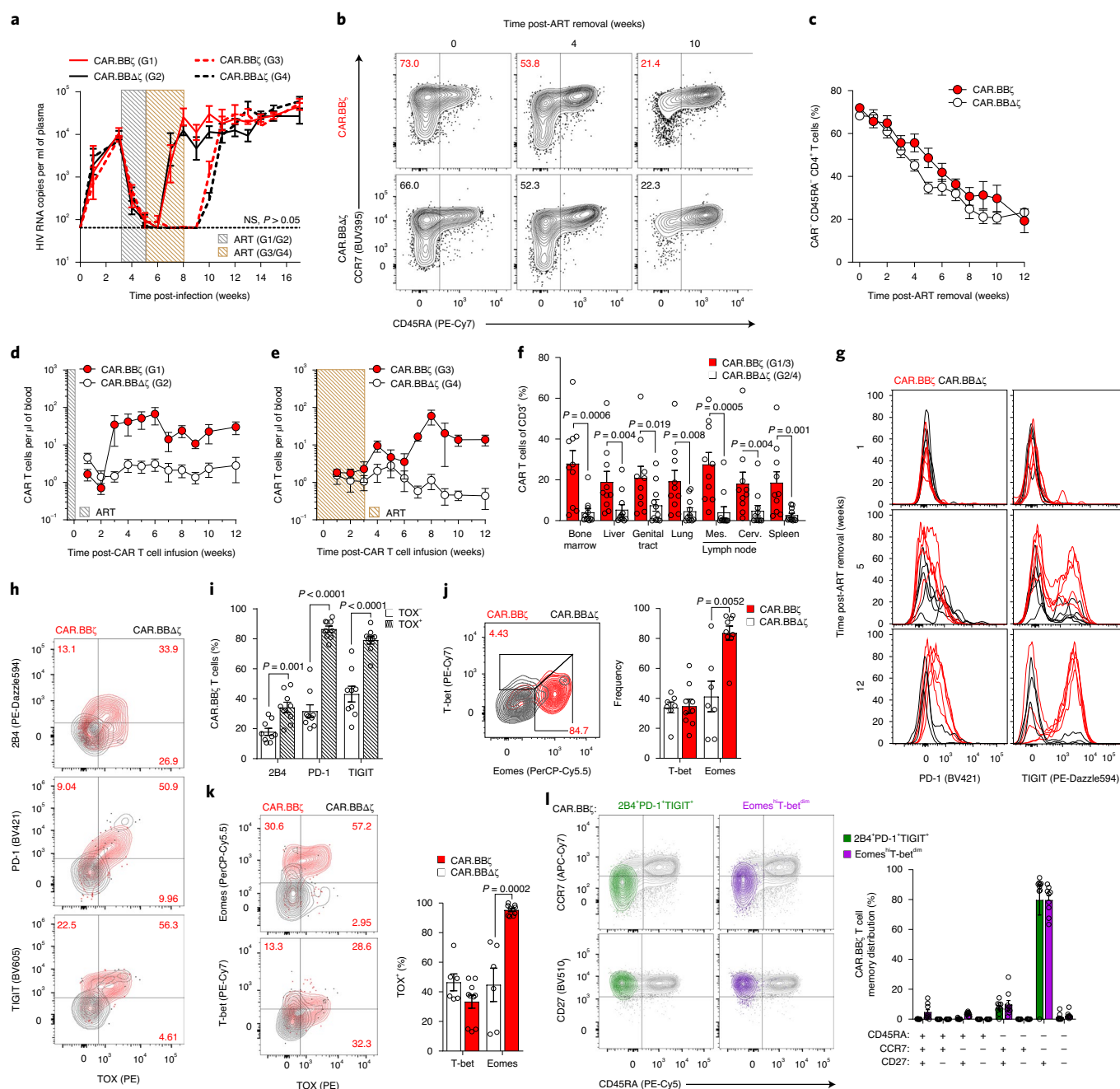


Fig. 3 | HIV-specific CAR.BB ζ T cells display features of T cell exhaustion after failing to control viral rebound. **a**, Mean log plasma viral RNA (copies per milliliter) in HIV_{JRC5F}-infected mice treated with ART from week 3 to 5 (G1 and G2 mice; gray box) or from week 3 to 8 (G3 and G4 mice; brown box). At 5 weeks post-infection, mice in G1 ($n=6$) and G3 ($n=10$) received 10^7 CAR.BB ζ T cells, and mice in G2 ($n=6$) and G4 ($n=9$) received 10^7 inactive control CAR.BB $\Delta\zeta$ T cells. Thin, dotted line denotes limit of quantification. Sample sizes in these studies indicate biologically independent animals. **b, c**, FACS plots (**b**) and summary data (**c**) illustrate the frequency of total memory CD4⁺ T cells (CAR⁻) following ART cessation in CAR.BB ζ and CAR.BB $\Delta\zeta$ T cell-treated mice. **d, e**, Concentration of peripheral CAR T cells for G1/G2 (**d**) and G3/G4 (**e**). **f**, Frequency of CAR T cells in tissues at 12 weeks post-CAR T cell infusion for G1/G3 and G2/G4. **g**, PD-1 and TIGIT expression on peripheral CAR.BB ζ or CAR.BB $\Delta\zeta$ T cells from G1/G2 after ART discontinuation. **h–i**, FACS analysis of splenic tissue of BLT mice (G1 and G2) 12 weeks after ART cessation. **h**, Coexpression of TOX and 2B4, PD-1 or TIGIT on peripheral CAR.BB ζ or CAR.BB $\Delta\zeta$ T cells. **i**, Frequency of TOX⁻ and TOX⁺ CAR.BB ζ T cells positive for indicated inhibitory receptors. **j**, Frequency of T-bet⁻ and Eomes-expressing CAR.BB ζ and CAR.BB $\Delta\zeta$ T cells. **k**, Frequency of TOX expression within T-bet⁺ and Eomes⁺ CAR.BB ζ and CAR.BB $\Delta\zeta$ T cells. **l**, Memory distribution of 2B4⁺PD-1⁺TIGIT⁺ and Eomes^{hi}T-bet^{dim} CAR.BB ζ T cells. For all data, symbols and bars reflect mean and error bars indicate \pm s.e.m., except **f** and **i–l** where symbols represent individual mice. In **a**, **f** and **i–k**, significance was calculated using a two-sided Wilcoxon rank-sum test. Cerv., cervical; Mes., mesenteric; NS, not significant.

probabilities, the Dual-CAR TCP comprises three populations: CAR.BB ζ , CAR.28 ζ and Dual-CAR T cells, the last of which simultaneously expresses both CD4-based CARs (Fig. 4a). Inclusion of the CD28-costimulated CAR increased in vitro cytokine production

of Dual-CAR T cells over CAR.BB ζ T cells (Supplementary Fig. 5). To evaluate the Dual-CAR TCP in vivo, we used an acute infection model in which mice received CAR T cells 48 h after HIV_{JRC5F} challenge to provide a more rapid model to test therapeutic efficacy.

Although we observed no differences in acute viremia between the Dual-CAR TCP-treated and untreated groups (Fig. 4b), CAR T cell-treated mice exhibited a significant, albeit transient, delay in the loss of peripheral memory CD4⁺ T cells (CAR⁻), which coincided with peak expansion of total CAR T cells in peripheral blood (Fig. 4b,c and Extended Data Fig. 4a). Notably, this delay in CD4⁺ T cell loss was observed in central, transitional and effector memory subsets (Extended Data Fig. 4b), an effect that was not observed after ART discontinuation in the CAR.BBζ-treated mice in the previous study (Fig. 3b,c).

We next assessed the efficacy of the Dual-CAR TCP in the context of a more physiologically relevant strain of HIV. To do so, we infected additional mice from the same cohort as above with HIV_{MJ4}, which exhibits slower acute-phase replication kinetics than HIV_{JRCSF} but ultimately achieves equivalent set-point viremia (Supplementary Fig. 6). Although the infusion of CAR T cells 48 h post-infection, again, did not alter viremia (Fig. 4d), we now observed more profound CD4⁺ T cell preservation and maintenance of the Dual-CAR TCP in peripheral blood as compared with the CAR T cell-treated mice infected with HIV_{JRCSF} (Fig. 4e,f and Extended Data Fig. 5a). The preservation of CD4⁺ T cells was particularly accentuated in transitional and effector memory populations, which express greater levels of CCR5 (Extended Data Fig. 5b). Similarly, the percentages of all memory CD4⁺ T cell subsets in the tissues at necropsy were substantially preserved in Dual-CAR TCP-treated compared with untreated HIV_{MJ4}-infected mice (Fig. 4f and Extended Data Fig. 5c), whereas there was no difference between CAR T cell-treated and control HIV_{JRCSF}-infected mice (Fig. 4f and Extended Data Fig. 4c). Thus, treatment with the Dual-CAR TCP can effectively limit HIV-induced depletion of memory CD4⁺ T cells, an effect that is modulated by the pathogenicity of the infecting virus.

Dual-CAR T cells exhibit vigorous in vivo proliferation in a competitive environment. The linkage of each CAR to a unique fluorescent protein allowed for independent quantification of each CAR T cell type within the Dual-CAR TCP and revealed increased in vivo expansion of Dual-CAR T cells relative to either of the single costimulatory domain-expressing CAR T cells (Fig. 4g). Notably, significant differences were observed in the peak expansion and cumulative proliferation of Dual-CAR T cells (Fig. 4h,i), which remained significant after correcting for the baseline absolute count of each population (Extended Data Fig. 6a). In addition, we compared the proliferative capacity of Dual-CAR T cells with third-generation (3G)-CAR T cells, which express CD28 and 4-1BB linearly in the same construct (Extended Data Fig. 6b). Here we combined an equal amount of Dual-CAR and 3G-CAR T cells before adoptive transfer into recipient mice (Extended Data Fig. 6c). After infusion, Dual-CAR T cells showed significantly greater

antigen-independent engraftment (Extended Data Fig. 6d), and also demonstrated superior antigen-driven proliferation after infusion of K.Env cells (Extended Data Fig. 6e). In contrast, 3G-CAR T cells marginally expanded and then progressively declined. Notably, during HIV_{MJ4} infection, Dual-CAR T cells exhibited profound proliferation (Fig. 4j,k) and long-term survival (Fig. 4l,m) relative to 3G-CAR T cells within the same mice. Together, these studies reveal the striking proliferative capacity exhibited by Dual-CAR T cells in a competitive setting under both antigen scarce and abundant in vivo environments.

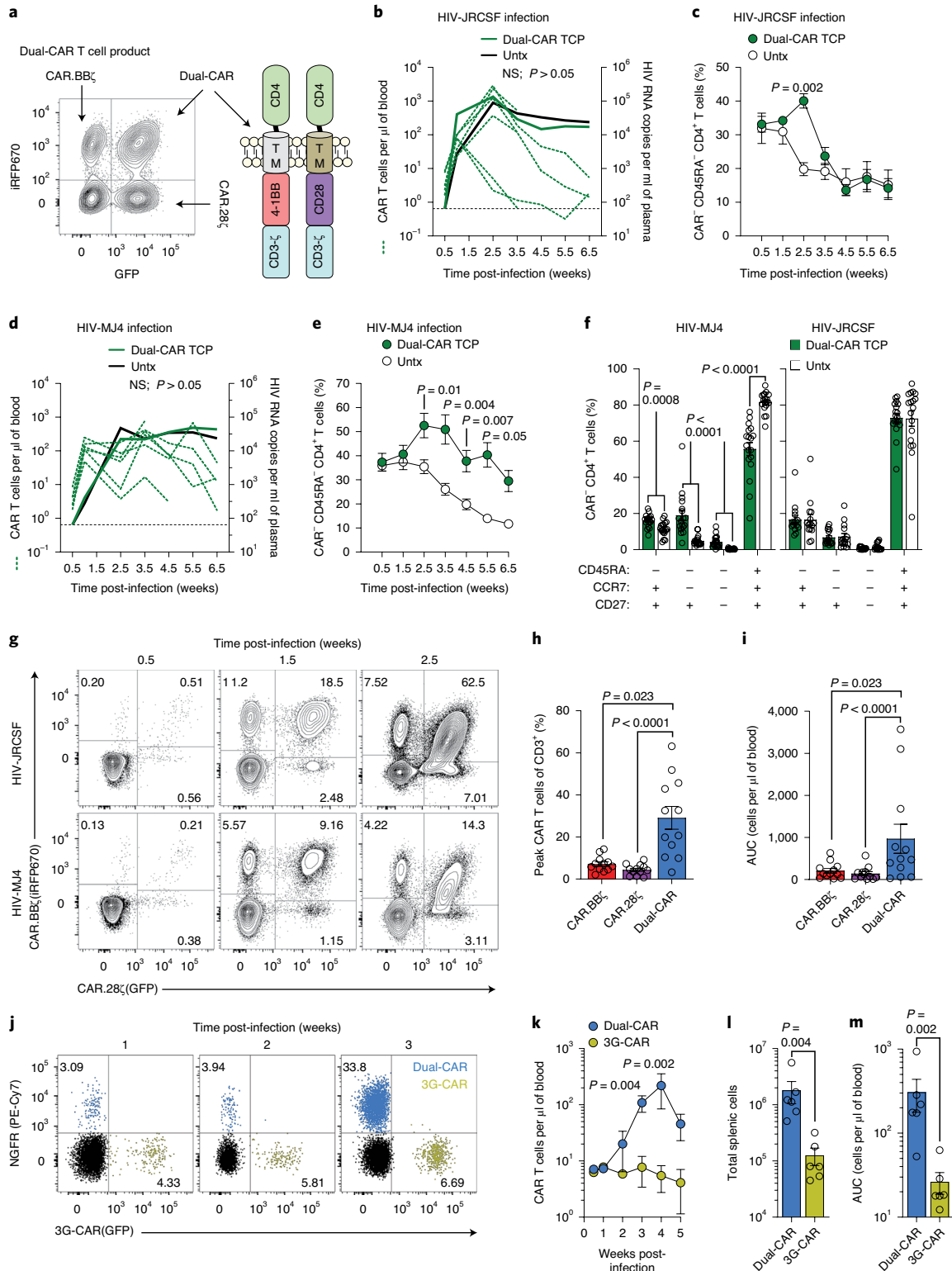
Engineering HIV resistance augments CAR T cell persistence and function. Despite the ability of CD4-based CARs to more efficiently suppress in vitro HIV replication versus several HIV-specific antibody-based CARs²⁶, and the reduced likelihood for viral escape due to the requirement for HIV to bind CD4 for infection, this CAR results in the over-expression of the CD4 extracellular domain on the T cell surface, potentially increasing susceptibility to infection. Indeed, HIV-infected CAR T cells were detected in vivo, although the extent of total infection appeared to be indistinguishable from endogenous CAR⁻ T cells (Supplementary Fig. 7a,b). More importantly, ex vivo stimulation revealed functional deficits in the capacity of HIV-infected CAR T cells to couple granzyme B and perforin (Supplementary Fig. 7c,d). To confer HIV resistance, we cotransduced the Dual-CAR TCP with the surface-expressed HIV fusion inhibitor C34-CXCR4 (ref. 44) (Fig. 5a and Supplementary Fig. 8a). C34-CXCR4 was expressed on up to 50% of cells in the Dual-CAR TCP and provided protective benefit as the C34-CXCR4⁺ CAR T cells harbored significantly less HIV DNA than their unprotected counterparts (Fig. 5b), and were selected for over time in chronically infected mice (Extended Data Fig. 7a,b). Importantly, C34-CXCR4⁺ CAR T cells from chronic infection had markedly improved cytotoxic potential and MIP-1β expression relative to unprotected CAR T cells within the same mice (Extended Data Fig. 7c,d). Somewhat paradoxically, however, infusion of a Dual-CAR TCP where 50% of all cells were HIV-resistant was still insufficient to reduce acute virus replication (Supplementary Fig. 8b). These results demonstrate that CD4-based CAR T cells can be protected from HIV infection by the C34-CXCR4 fusion inhibitor and that such protection can preserve CAR T cell functionality during persistent exposure to HIV.

HIV-resistant Dual-CAR T cells are responsible for mitigating HIV-induced CD4⁺ T cell loss. To determine whether an infusion product of Dual-CAR T cells alone exhibits enhanced virus-specific responses during HIV infection, we infused a low dose of C34-CXCR4⁺, purified Dual-CAR T cells, CAR.BBζ or CAR.28ζ T cells into separate groups of HIV_{MJ4}-infected mice. Dual-CAR

Fig. 4 | Dual-CAR TCP mitigates CD4⁺ T cell loss and exhibits superior proliferative capacity. a–i, Mice were challenged with HIV_{JRCSF} ($n=12$) or HIV_{MJ4} ($n=12$) and 48 h later six mice from each group were infused with Dual-CAR TCP (green lines) or were untreated (Untx, black lines). **a**, Dual-CAR TCP comprises CAR.BBζ, CAR.28ζ and Dual-CAR T cells. **b**, Concentration of total peripheral CAR T cells in individual mice (green dotted lines; left y axis) and mean log plasma viral RNA (copies per milliliter) (solid lines; right y axis) in HIV_{JRCSF}-infected mice. Thin black dotted line denotes limit of quantification. **c**, Frequency of peripheral memory CD4⁺ T cells (CAR⁻) in HIV_{JRCSF}-infected mice. **d**, Concentration of total peripheral CAR T cells in individual mice (green dotted lines; left y axis) and mean log plasma viral RNA (copies per milliliter) (solid lines; right y axis) in HIV_{MJ4}-infected mice. Thin black dotted line denotes limit of quantification. **e**, Frequency of peripheral memory CD4⁺ T cells (CAR⁻) in HIV_{MJ4}-infected mice. **f**, Frequency of CD4⁺ T cell (CAR⁻) memory subsets in tissue from HIV_{MJ4}- (left) HIV_{JRCSF}-infected mice (right) at 8 weeks post-CAR T cell infusion. Six distinct tissues were analyzed from three biologically independent animals per infection cohort. **g**, Peripheral longitudinal frequency of each CAR T cell type present in the Dual-CAR TCP. **h,i**, Peak peripheral frequency (**h**) and cumulative persistence (**i**) of CAR T cells. Data are aggregated from both infection cohorts ($n=12$). **j–m**, Equal frequencies of Dual-CAR TCP and 3G CD4-based CAR T cells were combined (Extended Data Fig. 6c) before infusion into HIV_{MJ4}-infected mice ($n=6$). **j**, Overlaid FACS plots showing frequency of peripheral Dual-CAR (iRFP670⁺NGFR⁺) and 3G-CAR (GFP⁺) T cells within the same mouse. **k**, Concentration of peripheral CAR T cells. **l,m**, Total number of splenic CAR T cells (**l**) and cumulative CAR T cell persistence (**m**) at 5 weeks post-infection. For all data, bars and error bars show mean \pm s.e.m., and symbols represent individual mice, except **c** and **e** where symbols represent mean. Two-sided Wilcoxon rank-sum test was used to calculate significance, except **h** and **i** where Friedman's test with Dunn's multiple corrections test was used. Sample sizes in these studies indicate biologically independent animals.

T cells exhibited notable *in vivo* expansion kinetics that exceeded both single CAR-transduced T cell populations (Fig. 5c,d), and mitigated HIV-induced CCR5⁺ CD4⁺ T cell loss (Supplementary Fig. 9). However, to more stringently control for CAR surface expression we performed an additional study in another cohort of mice where HIV-resistant, purified Dual-CAR T cells were compared with HIV-resistant, purified CAR T cells transduced with two independent CAR.BBζ or CAR.28ζ constructs (Supplementary Fig. 10).

Dual-CAR T cells again demonstrated remarkable sensitivity to acute virus replication, expanding 300-fold to represent 30% of total human cells in blood 3 weeks post-infection, whereas CAR.BBζ, BBζ and CAR.28ζ.28ζ T cells reached only 3% and 1%, respectively (Fig. 5e and Supplementary Fig. 11a). In addition, Dual-CAR T cells sustained greater long-term proliferation and maintenance in blood and tissues than CAR.28ζ.28ζ or CAR.BBζ.BBζ T cells (Fig. 5f,g and Supplementary Fig. 11b). Importantly, the infusion of purified



Dual-CAR T cells resulted in the greatest protection against CD4⁺ T cell loss during HIV_{M14} infection (Fig. 5h–j), reflected in the preservation of total memory and CCR5⁺ CD4⁺ T cells especially late in the infection (Supplementary Fig. 11c,d). Furthermore, the magnitude of early CAR T cell expansion across all groups, but exemplified by Dual-CAR T cells, was positively correlated with CD4⁺ T cell preservation (Supplementary Fig. 11e). Together, these data indicate that after controlling for CAR surface expression, Dual-CAR T cells exhibit the greatest *in vivo* antiviral effect.

Ex vivo effector function of Dual-CAR T cells exceeds 4-1BB-costimulated CAR T cells. We next interrogated the *ex vivo* effector functions of CAR T cells from chronically infected mice. Dual-CAR T cells were superior to CAR.BBζ.BBζ T cells and equivalent to CAR.28ζ.28ζ T cells in their ability to produce MIP-1β and degranulate based on CD107a expression (Fig. 5k,l). Notably, a majority of CD107a⁺ Dual-CAR T cells coexpressed granzyme B and perforin compared with CAR.BBζ.BBζ T cells, indicating that these cells possess cytotoxic potential (Fig. 5m,n). In further support of cytolytic function, CAR T cells comprising the Dual-CAR TCP induced active caspase-3 expression in K.Env cells after *ex vivo* stimulation (Extended Data Fig. 8). Moreover, comparison of IL-2, TNF, MIP-1β and CD107a expression revealed distinct effector profiles between these CAR T cell populations (Extended Data Fig. 9a,b). Dual-CAR and CD28-costimulated CAR T cells clustered in a similar fashion, with CD4⁺ CAR T cells expressing more TNF and IL-2, and CD8⁺ CAR T cells upregulating more CD107a and MIP-1β. In contrast, CD4⁺ and CD8⁺ 4-1BB-costimulated CAR T cells clustered together and exhibited attenuated levels of effector molecules (Extended Data Fig. 9c). Together, these findings support our hypothesis that Dual-CAR T cells harness both the antigen-driven proliferation and effector functions mediated by 4-1BB and CD28 costimulation, respectively, for improved potency.

Protecting CAR T cells from HIV infection improves control over virus replication. We hypothesized that the contribution of HIV-infected CAR T cells to viremia may be significant, in that virus secreted from infected CAR T cells could mask reductions in viral load caused by clearing infected CD4⁺ T cells. Indeed, after aggregating the data from all infection studies, we observed that infusion of HIV-susceptible CAR T cells significantly magnifies plasma viremia (Fig. 6a), as well as viral burden in tissues (Extended Data Fig. 10a,b). Thus, to test whether HIV infection of CD4-based CAR T cells negates CAR T cell-mediated reductions in viremia, we compared the outcomes of infusing a fully protected (>98% C34-CXCR4⁺) or a partially protected (<20% C34-CXCR4⁺) Dual-CAR TCP into HIV_{M14}-infected, ART-suppressed mice followed by ART cessation. Strikingly, infusion of the partially protected Dual-CAR TCP increased rebound viremia over untreated mice to an average peak rebound of 4.6 log HIV RNA copies per ml versus 3.8 log copies per ml, whereas the fully protected Dual-CAR

TCP significantly reduced viral load to 3.0 log copies per ml (Extended Data Fig. 10c). We confirmed this result by infusing the fully protected, Dual-CAR TCP into a larger cohort of BLT mice and observed significant reductions in acute viremia compared with untreated mice (Fig. 6b). Notably, treatment with the C34-CXCR4⁺ Dual-CAR TCP reduced the frequency of HIV-infected cells in tissues (Fig. 6c,d), contrasting the effect of unprotected CAR T cells on tissue viral burden in viremic mice (Extended Data Fig. 10a,b). Together, these data demonstrate the importance of safeguarding CAR T cells as HIV infection of unprotected CAR T cells can contribute to plasma viremia and potentially overwhelm CAR T cell-mediated control over virus replication.

Although C34-CXCR4 reduces HIV infection of CAR T cells, we have shown that the protection is not sterilizing in the presence of persistent viremia (Fig. 5b). To test whether providing ART to prevent new rounds of infection at the time of CAR T cell infusion could further reveal CAR T cell-mediated viral load reduction, we challenged mice with HIV_{JRC5F} and initiated combination therapy (ART and Dual-CAR TCP) at peak viremia. After 1 week of combination therapy, the Dual-CAR TCP-treated mice achieved approximately a 1-log greater reduction in viral load relative to the ART-only control group, which corresponded to a 50% reduction in viremia from pretreatment levels (Fig. 6e,f). We confirmed the suppressive effect of the Dual-CAR TCP in a separate cohort of mice infected with a different HIV strain (HIV_{BAL}) (Extended Data Fig. 10d,e). Aggregation of the data from the two studies showed that the magnitude of early viral load reduction was associated with the contemporaneous concentration of CAR T cells in peripheral blood (Fig. 6g), and that CAR T cell treatment significantly accelerated HIV suppression, with nearly all combination therapy-treated mice reaching full suppression by 2 weeks after treatment initiation versus 4 weeks for ART-treated control mice (Fig. 6h). Furthermore, the Dual-CAR TCP reduced tissue viral burden in mice with suppressed plasma viremia, evidenced by fewer HIV-infected CD8⁻ T cells (CAR⁻) and CD14⁺ macrophages in the tissues (Fig. 6i,j). Notably, central memory CD4⁺ T cells (CAR⁻) sorted from mice treated with the Dual-CAR TCP exhibited a significant, albeit modest, reduction in cell-associated HIV DNA load compared with the control group (Fig. 6k), suggesting that CAR T cell therapy is capable of reducing the size of the virus reservoir that forms during ART. Together, these findings highlight the potential for the HIV-resistant Dual-CAR TCP to mediate direct antiviral activity to clear infected cells *in vivo*.

Discussion

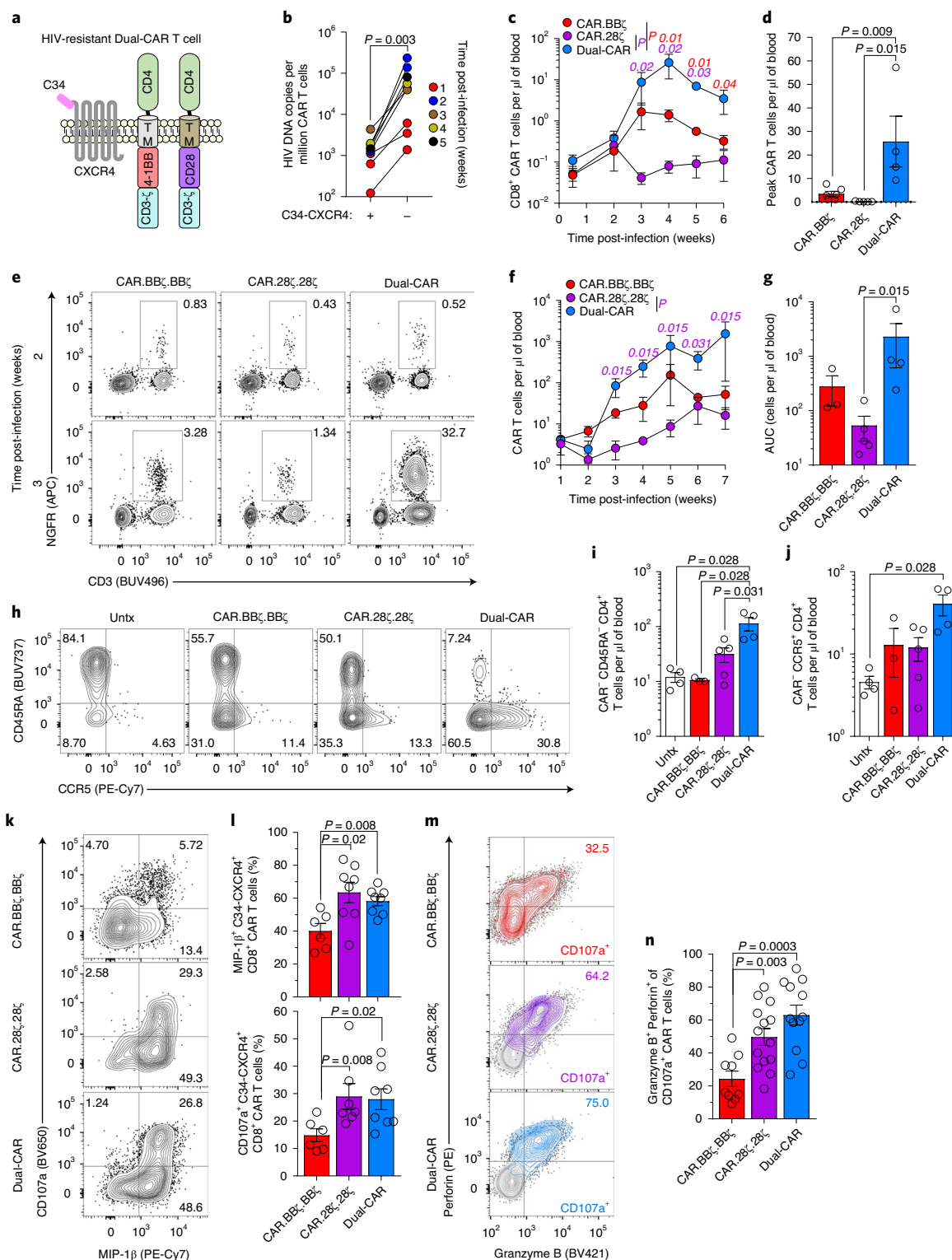
Here we use the BLT humanized mouse model to iteratively develop a CD4-based CAR T cell treatment of HIV infection. Although, initially, 4-1BB-costimulated CAR T cells demonstrated marked *in vivo* antigen-driven proliferation and survival, they failed to control viremia after ART cessation. To increase effector function, we created a Dual-CAR T cell that simultaneously expresses two CD4-based CARs independently encoding 4-1BB/CD3-ζ and CD28/CD3-ζ

Fig. 5 | HIV-resistant Dual-CAR T cells mediate superior virus-specific immune responses. **a**, Schematic of HIV-resistant (C34-CXCR4⁺) Dual-CAR T cells. **b**, HIV_{JRC5F}-infected BLT mice received 10⁷ CAR T cells at 48 h postchallenge. HIV DNA load in sorted CAR T cells from individual mouse splenic tissue (*n* = 8). **c,d**, HIV_{M14}-infected mice were infused at 48 h postchallenge with 10⁶ C34-CXCR4⁺, CAR.BBζ (*n* = 6), CAR.28ζ (*n* = 5) or purified Dual-CAR (*n* = 4) T cells. Longitudinal peripheral concentration (**c**) and peak peripheral CAR T cell concentration (**d**). **e–n**, HIV_{M14}-infected mice were infused at 48 h postchallenge with 10⁶ C34-CXCR4⁺, purified CAR.BBζ.BBζ (*n* = 5), CAR.28ζ.28ζ (*n* = 5) or Dual-CAR (*n* = 5) T cells, or were untreated (*n* = 4). Purification strategy is described in Supplementary Fig. 10. **e**, Frequency of CAR T cell populations out of total human CD45⁺ cells 2 and 3 weeks post-infection. **f,g**, Longitudinal concentration (**f**) and cumulative peripheral CAR T cell persistence (**g**). **h**, FACS plots showing CCR5 expression within peripheral memory CD4⁺ T cells (CAR⁻). **i,j**, Concentration of total memory (**i**) and CCR5⁺ (**j**) CD4⁺ T cells (CAR⁻) at 6 weeks post-infection. **k,l**, FACS plots (**k**) and frequency (**l**) of MIP-1β⁺ and CD107a⁺ CD8⁺ CAR T cells from tissue at 8 weeks post-infection after *ex vivo* stimulation. **m,n**, Distribution (**m**) and frequency (**n**) of granzyme B⁺ perforin⁺ cells within CD107a⁺ CAR T cells from tissues after *ex vivo* stimulation. **b**, Two-sided Wilcoxon matched-pairs signed rank test was used to calculate significance. For remaining analyses, significance was calculated using a two-sided Wilcoxon rank-sum test. Bars and error bars indicate mean ± s.e.m., and symbols represent individual mice, except for **c** where symbols indicate mean. Sample sizes in these studies indicate biologically independent animals.

endodomains. These Dual-CAR T cells exhibited both the cytotoxic potential and cytokine expression of CD28-costimulated CAR T cells and the proliferative capacity of 4-1BB-costimulated CAR T cells, suggesting concurrent contribution by both costimulatory signals. In contrast, 3G CD4-based CAR T cells exhibited the more limited expansion of CAR.28 ζ T cells despite containing a 4-1BB costimulatory domain within the same construct, likely the result of a dominant effect of the membrane-proximal CD28 domain as

described for 3G cancer-specific CAR T cells^{45–48}. This Dual-CAR approach introduces the potential to produce a CAR T cell with the benefits of both 4-1BB and CD28 costimulation.

The immunodeficiency caused by HIV infection is characterized by infection of CD4 T cells and concomitant immune activation and dysfunction⁴⁹. Importantly, the rapid antigen-driven proliferation of CAR T cells makes them susceptible to these same pathogenic mechanisms. In particular, the extracellular domain of CD4-based



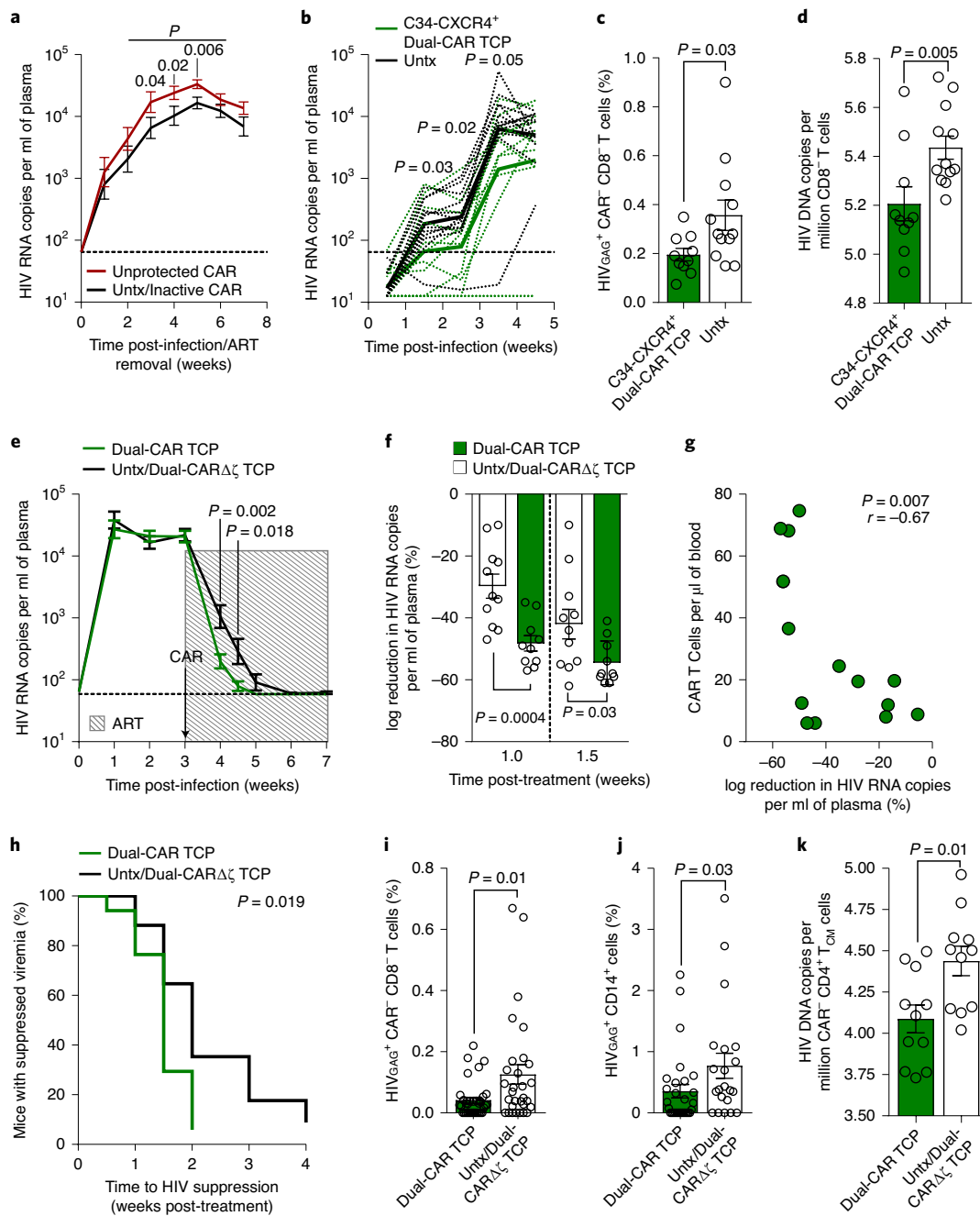


Fig. 6 | Mitigating CAR T cell infection improves control over HIV replication. **a**, Mean log plasma viral RNA (copies per milliliter) of active, unprotected CAR T cell-treated mice ($n=38$), and untreated/inactive CAR T cell-treated mice ($n=36$). Data are aggregated across six independent studies. Thin dotted line denotes limit of quantification. **b**, Mean log plasma viral RNA (copies per milliliter) in mice infused at 48 h post-HIV_{M14} challenge with 10^7 protected (>98% C34-CXCR4⁺) Dual-CAR TCP ($n=12$) or untreated mice ($n=12$). **c,d**, Frequency of splenic HIV-infected CD8⁻ T cells (CAR⁻) (**c**) and cell-associated HIV DNA load in lymph nodes (**d**) at 6–8 weeks post-infection. **e–k**, HIV_{RCSF}-infected mice were ART-treated and simultaneously infused with 10^7 HIV-resistant Dual-CAR TCP ($n=12$) or inactive Dual- Δ CAR TCP ($n=5$), or were untreated ($n=7$). **e**, Mean log plasma HIV RNA (copies per milliliter). Shaded box indicates ART and arrow indicates CAR TCP infusion. **f**, Percentage log reduction in plasma HIV RNA from pre-ART (week 3) to 1 and 1.5 weeks post-ART. **g,h**, Data are aggregated from HIV_{RCSF}- and HIV_{BAL}-infected cohorts. **g**, Correlation between percentage viral load reduction at first post-ART time-point and contemporaneous peripheral CAR T cell concentration. **h**, Kaplan–Meier curve of time to viral suppression after treatment initiation for Dual-CAR TCP versus control mice. **i,j**, Frequency of HIV-infected CD8⁻ T cells (CAR⁻) (**i**) and HIV-infected CD14⁺ macrophages (**j**) aggregated from various tissues of plasma viremia suppressed mice. **k**, Cell-associated HIV DNA load in sorted central memory (CAR⁻CD45RA⁻CCR7⁺) CD4⁺ T cells. Statistical significance was calculated by one-sided unpaired Student's *t*-test (**a** and **b**), two-sided Wilcoxon rank-sum test (**c–f** and **i–k**), Spearman correlation (**g**) and log-rank test (**h**). Bars and error bars indicate mean \pm s.e.m. Symbols represent individual mice. Sample sizes in these studies indicate biologically independent animals. *r*, coefficient of correlation.

CARs renders both CD4⁺ and CD8⁺ CAR T cells infectable, resulting in a substantial contribution to plasma viremia, as well as functional deficits. To combat this, we coexpressed a C34-CXCR4

(ref. 44) fusion inhibitor, which significantly improved CAR T cell survival and effector function during early HIV infection. Notably, the HIV-resistant Dual-CAR T cell treatment also resulted in a

reduction in HIV burden in a variety of tissues and cell types, including long-lived memory CD4⁺ T cells, which suggests for the first time that a CAR T cell therapy targeted the HIV reservoir. However, the benefit of C34-CXCR4 waned over time, which highlights the need to confer complete and permanent HIV resistance, perhaps through the deletion of CCR5 (refs. ^{50–53}).

The HIV-resistant Dual-CAR T cell treatment resulted in substantial protection of memory and CCR5⁺ CD4⁺ T cells from HIV-induced depletion despite failing to durably control viremia. Interestingly, the degree of protection was associated with the viral replication capacity (vRC) of the infecting strain. This is consistent with earlier findings that vRC affects many aspects of HIV-associated pathogenesis, including the kinetics of CD4⁺ T cell loss in acute infection⁵⁴. Since the vRC of transmitted/founder viruses can vary by orders of magnitude across infected individuals^{55–57}, vRC may become an important clinical consideration for the efficacy of CAR T cell treatment of HIV.

The HIV/BLT mouse model recapitulates key characteristics of HIV infection that are necessary to explore the efficacy of HIV-specific CAR T cell therapy. This small animal model may actually provide an overtly stringent test of CAR T cell efficacy given the general inability of BLT mice to develop affinity-matured antibodies^{58–60}. We have used this model to develop a Dual-CAR T cell that successfully exhibits the functionalities mediated by both CD28 and 4-1BB costimulation, and was capable of reducing viremia, limiting HIV-induced CD4⁺ T cell loss and diminishing viral tissue burden in the context of a fully disseminated infection. Collectively, these findings provide critical insight into the iterative development of an engineered T cell–based therapy for HIV and describe a product that not only mitigates HIV pathogenesis but also has broad utility for viral infections and malignancies.

Online content

Any methods, additional references, Nature Research reporting summaries, source data, extended data, supplementary information, acknowledgements, peer review information; details of author contributions and competing interests; and statements of data and code availability are available at <https://doi.org/10.1038/s41591-020-1039-5>.

Received: 27 January 2020; Accepted: 28 July 2020;

Published online: 31 August 2020

References

- June, C. H. & Sadelain, M. Chimeric antigen receptor therapy. *N. Engl. J. Med.* **379**, 64–73 (2018).
- Walker, B. & McMichael, A. The T-cell response to HIV. *Cold Spring Harb. Perspect. Med.* **2**, 1–19 (2012).
- Gross, G., Waks, T. & Eshhar, Z. Expression of immunoglobulin-T-cell receptor chimeric molecules as functional receptors with antibody-type specificity. *Proc. Natl Acad. Sci. USA* **86**, 10024–10028 (1989).
- van der Stegen, S. J., Hamieh, M. & Sadelain, M. The pharmacology of second-generation chimeric antigen receptors. *Nat. Rev. Drug Discov.* **14**, 499–509 (2015).
- Maude, S. L. et al. Chimeric antigen receptor T cells for sustained remissions in leukemia. *N. Engl. J. Med.* **371**, 1507–1517 (2014).
- Porter, D. L. et al. Chimeric antigen receptor T cells persist and induce sustained remissions in relapsed refractory chronic lymphocytic leukemia. *Sci. Transl. Med.* **7**, 303ra139 (2015).
- Brentjens, R. J. et al. Genetically targeted T cells eradicate systemic acute lymphoblastic leukemia xenografts. *Clin. Cancer Res.* **13**, 5426–5435 (2007).
- Song, D. G. et al. In vivo persistence, tumor localization, and antitumor activity of CAR-engineered T cells is enhanced by costimulatory signaling through CD137 (4-1BB). *Cancer Res.* **71**, 4617–4627 (2011).
- Carpenito, C. et al. Control of large, established tumor xenografts with genetically retargeted human T cells containing CD28 and CD137 domains. *Proc. Natl Acad. Sci. USA* **106**, 3360–3365 (2009).
- Milone, M. C. et al. Chimeric receptors containing CD137 signal transduction domains mediate enhanced survival of T cells and increased antileukemic efficacy in vivo. *Mol. Ther.* **17**, 1453–1464 (2009).
- Cheng, Z. et al. In vivo expansion and antitumor activity of coinfluent CD28- and 4-1BB-engineered CAR-T cells in patients with B cell leukemia. *Mol. Ther.* **26**, 976–985 (2018).
- Quintarelli, C. et al. Choice of costimulatory domains and of cytokines determines CAR T-cell activity in neuroblastoma. *Oncoimmunology* **7**, e1433518 (2018).
- Kawalekar, O. U. et al. Distinct signaling of coreceptors regulates specific metabolic pathways and impacts memory development in CAR T cells. *Immunity* **44**, 380–390 (2016).
- Neelapu, S. S. et al. Axicabtagene ciloleucel CAR T-cell therapy in refractory large B-cell lymphoma. *N. Engl. J. Med.* **377**, 2531–2544 (2017).
- Park, J. H. et al. Long-term follow-up of CD19 CAR therapy in acute lymphoblastic leukemia. *N. Engl. J. Med.* **378**, 449–459 (2018).
- Salter, A. I. et al. Phosphoproteomic analysis of chimeric antigen receptor signaling reveals kinetic and quantitative differences that affect cell function. *Sci. Signal.* **11**, eaat6753 (2018).
- Schuster, S. J. et al. Tisagenlecleucel in adult relapsed or refractory diffuse large B-cell lymphoma. *N. Engl. J. Med.* **380**, 45–56 (2019).
- Abate-Daga, D. & Davila, M. L. CAR models: next-generation CAR modifications for enhanced T-cell function. *Mol. Ther. Oncolytics* **3**, 16014 (2016).
- Weinkove, R., George, P., Dasyam, N. & McLellan, A. D. Selecting costimulatory domains for chimeric antigen receptors: functional and clinical considerations. *Clin. Transl. Immunol.* **8**, e1049 (2019).
- Deeks, S. G. et al. A phase II randomized study of HIV-specific T-cell gene therapy in subjects with undetectable plasma viremia on combination antiretroviral therapy. *Mol. Ther.* **5**, 788–797 (2002).
- Colovos, C., Villena-Vargas, J. & Adusumilli, P. S. Safety and stability of retrovirally transduced chimeric antigen receptor T cells. *Immunotherapy* **4**, 899–902 (2012).
- Scholler, J. et al. Decade-long safety and function of retroviral-modified chimeric antigen receptor T cells. *Sci. Transl. Med.* **4**, 132ra153 (2012).
- Kim, G. B., Hege, K. & Riley, J. L. CAR talk: how cancer-specific CAR T cells can instruct how to build CAR T cells to cure HIV. *Front. Immunol.* **10**, 2310 (2019).
- Ali, A. et al. HIV-1-specific chimeric antigen receptors based on broadly neutralizing antibodies. *J. Virol.* **90**, 6999–7006 (2016).
- Hale, M. et al. Engineering HIV-resistant, anti-HIV chimeric antigen receptor T cells. *Mol. Ther.* **25**, 570–579 (2017).
- Leibman, R. S. et al. Supraphysiologic control over HIV-1 replication mediated by CD8 T cells expressing a re-engineered CD4-based chimeric antigen receptor. *PLoS Pathog.* **13**, e1006613 (2017).
- Zhen, A. et al. Long-term persistence and function of hematopoietic stem cell-derived chimeric antigen receptor T cells in a nonhuman primate model of HIV/AIDS. *PLoS Pathog.* **13**, e1006753 (2017).
- Anthony-Gonda, K. et al. Multispecific anti-HIV duoCAR-T cells display broad in vitro antiviral activity and potent in vivo elimination of HIV-infected cells in a humanized mouse model. *Sci. Transl. Med.* **11**, eaav5685 (2019).
- Herzig, E. et al. Attacking latent HIV with convertible CAR-T cells, a highly adaptable killing platform. *Cell* **179**, e810 (2019).
- Sun, Z. et al. Intra-rectal transmission, systemic infection, and CD4⁺ T cell depletion in humanized mice infected with HIV-1. *J. Exp. Med.* **204**, 705–714 (2007).
- Denton, P. W. et al. Antiretroviral pre-exposure prophylaxis prevents vaginal transmission of HIV-1 in humanized BLT mice. *PLoS Med.* **5**, e16 (2008).
- Brainard, D. M. et al. Induction of robust cellular and humoral virus-specific adaptive immune responses in human immunodeficiency virus-infected humanized BLT mice. *J. Virol.* **83**, 7305–7321 (2009).
- Zhen, A. et al. Targeting type I interferon-mediated activation restores immune function in chronic HIV infection. *J. Clin. Invest.* **127**, 260–268 (2017).
- Boritz, E. A. et al. Multiple origins of virus persistence during natural control of HIV infection. *Cell* **166**, 1004–1015 (2016).
- Estes, J. D. et al. Defining total-body AIDS-virus burden with implications for curative strategies. *Nat. Med.* **23**, 1271–1276 (2017).
- Ventura, J. D. et al. Longitudinal bioluminescent imaging of HIV-1 infection during antiretroviral therapy and treatment interruption in humanized mice. *PLoS Pathog.* **15**, e1008161 (2019).
- Alfei, F. et al. TOX reinforces the phenotype and longevity of exhausted T cells in chronic viral infection. *Nature* **571**, 265–269 (2019).
- Khan, O. et al. TOX transcriptionally and epigenetically programs CD8⁺ T cell exhaustion. *Nature* **571**, 211–218 (2019).
- Scott, A. C. et al. TOX is a critical regulator of tumour-specific T cell differentiation. *Nature* **571**, 270–274 (2019).
- Seo, H. et al. TOX and TOX2 transcription factors cooperate with NR4A transcription factors to impose CD8⁺ T cell exhaustion. *Proc. Natl Acad. Sci. USA* **116**, 12410–12415 (2019).
- Yao, C. et al. Single-cell RNA-seq reveals TOX as a key regulator of CD8⁺ T cell persistence in chronic infection. *Nat. Immunol.* **20**, 890–901 (2019).
- Appay, V. et al. Memory CD8⁺ T cells vary in differentiation phenotype in different persistent virus infections. *Nat. Med.* **8**, 379–385 (2002).

43. Buggert, M. et al. T-bet and Eomes are differentially linked to the exhausted phenotype of CD8⁺ T cells in HIV infection. *PLoS Pathog.* **10**, e1004251 (2014).
44. Leslie, G. J. et al. Potent and broad inhibition of HIV-1 by a peptide from the gp41 heptad repeat-2 domain conjugated to the CXCR4 amino terminus. *PLoS Pathog.* **12**, e1005983 (2016).
45. Zhao, Z. et al. Structural design of engineered costimulation determines tumor rejection kinetics and persistence of CAR T cells. *Cancer Cell* **28**, 415–428 (2015).
46. Guedan, S. et al. Enhancing CAR T cell persistence through ICOS and 4-1BB costimulation. *JCI Insight* **3**, e96976 (2018).
47. Pule, M. A. et al. A chimeric T cell antigen receptor that augments cytokine release and supports clonal expansion of primary human T cells. *Mol. Ther.* **12**, 933–941 (2005).
48. Hombach, A. A., Heiders, J., Foppe, M., Chmielewski, M. & Abken, H. OX40 costimulation by a chimeric antigen receptor abrogates CD28 and IL-2 induced IL-10 secretion by redirected CD4⁺ T cells. *Oncoimmunology* **1**, 458–466 (2012).
49. Moir, S., Chun, T. W. & Fauci, A. S. Pathogenic mechanisms of HIV disease. *Annu. Rev. Pathol.* **6**, 223–248 (2011).
50. Perez, E. E. et al. Establishment of HIV-1 resistance in CD4⁺ T cells by genome editing using zinc-finger nucleases. *Nat. Biotechnol.* **26**, 808–816 (2008).
51. Holt, N. et al. Human hematopoietic stem/progenitor cells modified by zinc-finger nucleases targeted to CCR5 control HIV-1 in vivo. *Nat. Biotechnol.* **28**, 839–847 (2010).
52. Tebas, P. et al. Gene editing of CCR5 in autologous CD4 T cells of persons infected with HIV. *N. Engl. J. Med.* **370**, 901–910 (2014).
53. Peterson, C. W. et al. Differential impact of transplantation on peripheral and tissue-associated viral reservoirs: implications for HIV gene therapy. *PLoS Pathog.* **14**, e1006956 (2018).
54. Claiborne, D. T. et al. Replicative fitness of transmitted HIV-1 drives acute immune activation, proviral load in memory CD4⁺ T cells, and disease progression. *Proc. Natl Acad. Sci. USA* **112**, E1480–E1489 (2015).
55. Wright, J. K. et al. Influence of Gag-protease-mediated replication capacity on disease progression in individuals recently infected with HIV-1 subtype C. *J. Virol.* **85**, 3996–4006 (2011).
56. Prince, J. L. et al. Role of transmitted Gag CTL polymorphisms in defining replicative capacity and early HIV-1 pathogenesis. *PLoS Pathog.* **8**, e1003041 (2012).
57. Deymier, M. J. et al. Heterosexual transmission of subtype C HIV-1 selects consensus-like variants without increased replicative capacity or interferon- α resistance. *PLoS Pathog.* **11**, e1005154 (2015).
58. Seung, E. & Tager, A. M. Humoral immunity in humanized mice: a work in progress. *J. Infect. Dis.* **208**(Suppl 2), S155–S159 (2013).
59. Martinez-Torres, F., Nochi, T., Wahl, A., Garcia, J. V. & Denton, P. W. Hypogammaglobulinemia in BLT humanized mice—an animal model of primary antibody deficiency. *PLoS ONE* **9**, e108663 (2014).
60. Karpel, M. E., Boutwell, C. L. & Allen, T. M. BLT humanized mice as a small animal model of HIV infection. *Curr. Opin. Virol.* **13**, 75–80 (2015).

Publisher's note Springer Nature remains neutral with regard to jurisdictional claims in published maps and institutional affiliations.

© The Author(s), under exclusive licence to Springer Nature America, Inc. 2020

Methods

Ethics. Anonymized human fetal tissue (gestational age of 17–19 weeks) was acquired with informed consent from healthy donors by Advanced Bioscience Resources, and used under Partners Healthcare Institutional Review Board-approved protocols. Humanized mouse experiments performed at the Ragon Institute and at the University of Pennsylvania were approved by the Massachusetts General Hospital and the University of Pennsylvania Institutional Animal Care and Use Committee under the approved protocols 2016N000483 and 805606, respectively. Animal studies were performed following the instructions detailed in the Guide for the Care and Use of Laboratory Animals of the National Institutes of Health. Purified CD3⁺ and CD4⁺ T cells from anonymous healthy human donors were obtained by the University of Pennsylvania Human Immunology Core/Centers for AIDS Research (CFAR) Immunology Core.

Humanized mice. Male and female NOD/SCID/IL2Rγ^{-/-} (NSG) mice (Jackson Laboratory) were maintained in pathogen-free facilities at the Ragon Institute of MGH, MIT and Harvard or the University of Pennsylvania. Microisolation cages were used to house mice, and mice were fed autoclaved food and water. Animal rooms were maintained at 72 ± 2 °F (22.2 ± 1.1 °C) and 30–70% relative humidity and were on a 12:12-h light/dark cycle. BLT humanized mice were generated at the Ragon Institute as previously described^{32,61,62}. Briefly, 6–8-week-old NSG mice were anesthetized and whole-body irradiated (2 Gy), followed by implantation with 1-mm³ fragments of human fetal liver and thymus tissue under the murine kidney capsule. Then, 10⁵ autologous fetal liver-derived CD34⁺ hematopoietic stem cells (HSCs) were injected intravenously within 6 h of transplantation. BLT humanized mice were also generated at the University of Pennsylvania as previously described⁶³. Briefly, 1–1.5 × 10⁵ human fetal liver-derived CD34⁺ HSCs were administered intravenously into 7–10-week-old NSG mice 24 h after busulfan (30 mg kg⁻¹) conditioning. At 3–6 d following stem cell transplant, mice were surgically implanted with 3–5 fragments of autologous human fetal thymus tissue measuring 3–5 mm³ under the murine kidney capsule. For all BLT humanized mice, human immune reconstitution was assessed from 12 to 17 weeks after transplantation. Mice were included in experiments when over 50% of cells in the lymphocyte gate were positive for human CD45 and, of those human cells, greater than 40% were CD3⁺ T cells.

Flow cytometry and cell sorting. Washed cells were resuspended in 50 μl of PBS containing 2 mM EDTA and 2% FCS, and then surface stained with anti-human antibodies from BioLegend: CD45 (HI30 and 2D1), CD19 (HIB19), CD3 (OKT3), CD45RA (HI100), CD27 (LG.3A10), CD8 (RPA-T8), CCR7 (G043H7), CCR5 (J418F1), CD4 (OKT4), CD271 (ME20.4), PD-1 (EH12.2H7), TIGIT (VSTM3), 2B4 (C1.7), CD107a (H4A3); BD Biosciences: CD45 (HI30), CD3 (UCHT1), CD8 (SK1), CD45RA (HI100), CCR7 (3D12); and R&D: Human EGFR (Cetuximab Biosimilar, Hu1). Live cells were identified through staining negative for Fixable Viability Dye eFlour 780 (eBioscience) or LIVE/DEAD Fixable Blue (Invitrogen). For the detection of intracellular proteins, the cells were treated with Cell Fixation & Cell Permeabilization Kit (Invitrogen) or True-Nuclear Transcription Factor Buffer Set (BioLegend) in accordance with the manufacturer's protocols with antibodies from: BioLegend: IL-2 (MQH-17H12), Perforin (B-D48); BD Biosciences: TNF (Mab11), IFN-γ (4S.B3), Granzyme B (GB11), MIP-1β (D21-1351), GM-CSF (BVD2-21C11), Active Caspase-3 (C92605); Beckman Coulter: HIV-1 Core Antigen (KC57); and eBioscience: T-bet (4B10), EOMES (WD1928), TOX (TXRX10). Flow cytometry data were acquired on BD LSR II, BD LSRFortessa and BD FACS Symphony instruments using BD FACSDiva Software v.8.0.1 (BD Biosciences). Data were analyzed using FlowJo software v.10 (TreeStar). Sorting of C34-CXCR4⁺ and C34-CXCR4⁻ CAR T cells for quantification of viral burden by digital-droplet PCR was performed by sorting live C34-CXCR4⁺ and C34-CXCR4⁻ CAR T cells from splenocytes after surface staining with the following Biolegend antibodies: CD45 (2D1), CD3 (OKT3), CD8 (RPA-T8), CD4 (OKT4). Living CAR T cells were identified by staining negative for Fixable Viability Dye eFlour 780 (Supplementary Fig. 12a). Sorting of endogenous central memory CD4⁺ T cell populations for quantification of viral burden by droplet-digital PCR (ddPCR) was performed by staining splenocytes with the following antibodies from BioLegend: anti-mouse CD45 (30-F11), anti-human CD45 (HI30), CD20 (2H7), CD14 (HCD14), CD56 (HCD56), CD3 (OKT3), CD4 (RPA-T4), CD8 (SK1), CCR7 (G043H7), CD45RA (HI100). Live cells were discriminated using LIVE/DEAD Fixable Blue (Invitrogen). FACSaria II (BD Biosciences) was used for all cell sorting (Supplementary Fig. 12b). A complete list of antibodies used including additional technical information for flow cytometry experiments can be found in the Nature Research Reporting Summary.

HIV inoculum preparation. Viral stocks of the molecular clones, HIV_{JRC5F} and HIV_{MJ4} were generated through transfections of HEK293T cells (ATCC: CRL-3216) and titered as previously described⁶⁴. HIV_{BAL} virus stocks were generated by passage in anti-CD3/CD28 Dynabead stimulated human CD4⁺ T cells as previously described²⁶.

Viral (HIV) load quantification. Peripheral blood plasma-derived HIV RNA was isolated using the QiaAmp Viral RNA Mini Kit (Qiagen). Quantitative RT-PCR

using the QuantiFast Syber Green RT-PCR kit (Qiagen) was used as previously described to measure viral loads⁶⁴. Data were collected on a LightCycler 480 System (Roche) or a ViiA 7 Real-Time PCR system (Applied Biosystems) using Lightcycler 480 software release 1.5.1.62 SP3 or ViiA 7 QuantStudio Real-Time PCR software v.1.3, respectively.

Plasmid construction. Amino acid sequences specific to the CD4-based CAR constructs containing the intracellular signaling domains: CD3-ζ, 4-1BB/CD3-ζ and CD28/CD3-ζ, are described elsewhere²⁶. Each CAR was amplified from its parent plasmid with 5'-CACGTCCTAGGATGGCCTTACCAGTG and 5'-GTGGTCGACTTATGCGCTCTGCTGAAC and inserted into the AvrII and SalI restriction enzyme sites of the pTRPE transfer plasmid downstream of GFP, mCherry or iRFP670, and an intervening T2A linker permits expression of both proteins. To construct the plasmids for CAR T cell selection, double-stranded DNA fragments (IDT) encoding NGFR (CD271)⁶⁵ and truncated EGFR⁶⁶ were custom synthesized, flanked with suitable restriction enzyme sites and cloned into the second position of the pTRPE plasmid preceded by the CAR-BBζ and CAR-28ζ gene and T2A linker. The C34-CXCR4 construct's sequence is denoted elsewhere⁶⁴. A previously described⁶⁷ Asp mutation (D97N) in CXCR4 was introduced to impair SDF-1 binding and limit receptor internalization.

Lentiviral production and transfection. Lentiviral particles were generated using packaging expression vectors that encode VSV or Cocal glycoprotein, HIV Rev and HIV Gag/Pol (pTRPE pVSV-g, pCocal-g, pTRPE.Rev and pTRPE g/p, respectively), and were synthesized using DNA 2.0 or ATUM. The packaging plasmids along with the appropriate pTRPE transfer vector were transfected into HEK293T cells using Lipofectamine 2000 (Life Technologies)^{26,68}. At 24 and 48 h after transfection, the HEK293T cell supernatant was collected, filtered through a 0.45-μm syringe-driven filter and then concentrated by ultracentrifugation for 2.5 h at 25,000 r.p.m. at 4 °C. The supernatant was aspirated and the virus pellet was resuspended in 800 μl of complete RPMI and stored at -80 °C.

Cell culture. For preparation of CAR T cells: de-identified human donor T cells were isolated by negative selection with RosetteSep Human CD3⁺ Enrichment Cocktails (Stem-Cell Technologies) following the manufacturer protocol. T cells from BLT humanized mice were purified by processing spleen, bone marrow and liver tissues into a single-cell suspension. Density gradient centrifugation using Lymphoprep (Stem-Cell Technologies) was used to isolate Mononuclear cells. Human CD2⁺ cells were purified by CD2 Microbeads (Miltenyi Biotec) per the manufacturer's protocol. T cells were placed in culture at 10⁶ cells per ml in either complete RPMI: RPMI 1640, 1% Penicillin-Streptomycin, 2 mM GlutaMax and 25 mM HEPES buffer from Life Technologies, and 10% FCS (Seradigm), or CTS OpTmizer T-Cell Expansion SFM (Gibco) with 1% Penicillin-Streptomycin, 2 mM GlutaMax and 25 mM HEPES buffer. T cell expansion medium was complemented with human IL-15 (5 ng ml⁻¹, Biolegend) and IL-7 (10 ng ml⁻¹, R&D). T cells were stimulated at a 3:1 (bead/cell) ratio with anti-CD3/CD28 Dynabeads (Life Technologies), and incubated at 37 °C, 5% CO₂ and 95% humidity. At 18 h after stimulation the medium was reduced by and replaced with 300 μl of the appropriate lentivirus supernatant for CAR transduction. At 5 d after T cell activation, magnetic separation was used to remove Dynabeads. Throughout CAR T cell manufacturing, medium was changed every second day, which spanned 8–10 d, or as needed to adjust cell counts to 0.5 × 10⁶ cells per ml.

Two-step immunomagnetic selection of CAR T cells during manufacturing: on day 4 after initial T cell activation, anti-CD3/CD28 Dynabeads were removed by magnetic bead separation. T cells were counted and then incubated at a 1:2 cell/bead ratio with CELLlection Biotin Binder Dynabeads (Life Technologies) conjugated to anti-EGFR (Cetuximab) antibody. Truncated EGFR⁺ T cells were isolated according to the manufacturer's protocol. The cell concentration was adjusted to 0.5 × 10⁶ cells per ml with medium and expanded as described in the preceding paragraph. At 7 d after initial activation, EGFR⁺ T cells were counted and incubated with CD271 Microbeads (Miltenyi Biotec) to positively select for NGFR⁺ T cells according to the manufacturer's instructions. The eluted fraction of T cells contained 85–95% EGFR⁺NGFR⁺ T cells. Before infusion into BLT mice, the T cells were cultured for an additional day at the adjusted cell concentration.

HIV treatment and ART discontinuation mouse model. For the study in Fig. 3, BLT humanized mice were administered 2 mg of medroxyprogesterone (McKesson) subcutaneously 1 week before intravaginal challenge with 20,000 tissue culture infectious dose 50 (TCID₅₀) HIV_{JRC5F} in 20-μl total volume. Then, 75–100 μl of blood was obtained through puncture of the retro-orbital sinus weekly to quantify viral load and immunophenotype circulating blood cells. At 3 weeks post-HIV challenge, all infected mice were administered daily intraperitoneal injections of ART consisting of 10 mg kg⁻¹ EFdA (4'-ethynyl-2-fluoro-2'-deoxyadenosine, LeadGen Labs) and 50 mg kg⁻¹ Dolutegravir (Sigma) for 1 week and then every second day thereafter. Following 2 weeks of ART, four treatment groups were defined based on normalization of plasma viral load, body weight and human reconstitution percentages. G1 (*n* = 6) and G3 (*n* = 10) are treatment groups that were infused with 10⁷ CAR-BBζ T cells, while G2 (*n* = 6) and G4 (*n* = 9) are control groups that were infused with 10⁷ CAR-BBΔζ T cells that express a

defective CD3- ζ endodomain. T cells were administered in a 300- μ l volume via tail vein injection. ART was interrupted immediately after adoptive T cell transfer for G1 and G2, while ART discontinuation was delayed for 3 weeks in G3 and G4. At necropsy, 17 weeks after HIV challenge, various tissues were collected to analyze the CAR T cells.

For the study described in Extended Data Fig. 10c, BLT humanized mice were infected via the intraperitoneal route with 20,000 TCID₅₀ HIV_{MJ4}. At 3 weeks post-infection, all mice received ART and an HIV-resistant (<20% C34-CXCR4⁺) Dual-CAR TCP ($n=7$), an HIV-resistant Dual-CAR TCP with further magnetic bead selection to obtain a >98% C34-CXCR4⁺ transfer product ($n=5$) or no CAR T cells ($n=9$). After plasma viremia was fully suppressed in all three groups, ART was discontinued and virus rebound was monitored via weekly blood draws from the retro-orbital sinus.

Acute HIV infection treatment model. BLT humanized mice were challenged with 20,000 TCID₅₀ HIV_{JRC5F} or HIV_{MJ4} via intraperitoneal injection. For the study comparing the replication capacity of HIV_{JRC5F} and HIV_{MJ4} (Fig. 4a–i): HIV_{JRC5F}-infected mice ($n=6$) and HIV_{MJ4}-infected mice ($n=6$) were infused with the Dual-CAR TCP consisting of 2×10^7 total CAR T cells. T cells were administered via tail vein injection 48 h after HIV challenge. Control mice that were infected with HIV_{JRC5F} ($n=5$) or HIV_{MJ4} ($n=6$) received no T cells. For the study comparing Dual-CAR T cells and 3G CD4-based CAR T cells: Dual-CAR TCP was combined with 3G-CAR T cells, normalizing the frequency of Dual-CAR and 3G-CAR T cells before infusion into mice. Nine HIV-uninfected mice were infused with this mixture, where each mouse received 2.5×10^6 Dual-CAR T cells and 2.5×10^6 3G-CAR T cells via tail vein injection. After 2 weeks, six mice were infused via intravenous injection with 10^7 irradiated K.Env cells and three mice received 10^7 irradiated wild-type K562 (K.WT) cells (Extended Data Fig. 6). Additional mice ($n=6$) were challenged with 20,000 TCID₅₀ HIV_{MJ4} and infused 48 h later with the same Dual-CAR TCP/3G-CAR T cell mixture described above (Fig. 4j–m). For the study in Fig. 5c, HIV_{MJ4}-infected mice were allocated into four groups. The groups were infused with 10^6 C34-CXCR4⁺, CAR.BB ζ ($n=6$), CAR.28 ζ ($n=5$) or purified Dual-CAR ($n=4$) T cells, while the remaining mice were untreated ($n=6$). For the study comparing purified Dual-CAR and double CAR-transduced BB ζ .BB ζ and 28 ζ .28 ζ T cell populations (Fig. 5f): HIV_{MJ4}-infected mice were distributed into four groups and normalized based upon body weight and the absolute count of CD4⁺ T cells in blood. The groups were infused with 10^6 C34-CXCR4⁺, purified CAR.BB ζ .BB ζ ($n=5$), CAR.28 ζ .28 ζ ($n=5$) or Dual-CAR ($n=5$) T cells via tail vein injection 48 h after HIV challenge. Control mice did not receive T cells ($n=5$). For the study evaluating efficacy of enriched C34-CXCR4⁺ (>98%) Dual-CAR T cells (Fig. 6b–d), HIV_{MJ4}-infected mice were divided into two groups that received 10^7 C34-CXCR4-enriched Dual-CAR TCP ($n=12$) or were untreated ($n=12$). In all studies mice were bled by retro-orbital puncture 1 d after adoptive T cell transfer, and then weekly thereafter until their respective endpoint and tissue collection.

CAR T cell therapy and ART model. In the study described in Fig. 6e, BLT humanized mice were challenged with 20,000 TCID₅₀ HIV_{JRC5F} via intraperitoneal injection. At 3 weeks post-HIV challenge, all infected mice were given low-dose ART consisting of 1 mg kg⁻¹ EFdA and 25 mg kg⁻¹ Dolutegravir every other day by intraperitoneal injection for 4 weeks. At the time of ART initiation, HIV-infected mice were allocated into three groups. Treated mice ($n=11$) were infused with an HIV-resistant (C34-CXCR4⁺) Dual-CAR TCP consisting of 10^7 total CAR T cells. Control mice were infused with either 10^7 total CAR T cells from the HIV-resistant Dual- Δ CAR TCP which expresses defective CD3- ζ signaling domains ($n=5$) or were untreated ($n=7$). The mice were euthanized and tissues were collected for analysis 7 weeks post-infection. For the study described in Extended Data Fig. 10d, BLT humanized mice were challenged with 20,000 TCID₅₀ HIV_{BAL} via intraperitoneal injection. At 3 weeks post-HIV challenge, all infected mice were administered ART consisting of 10 mg kg⁻¹ EFdA and 25 mg kg⁻¹ Dolutegravir every other day by intraperitoneal injection for 2 weeks. At the time of ART initiation, HIV-infected mice were distributed into two groups. Treated mice ($n=6$) were infused with an HIV-resistant (C34-CXCR4⁺) Dual-CAR TCP comprising 10^7 total CAR T cells, or were untreated ($n=6$).

C34-CXCR4 protection of CAR T cells in vivo. In Fig. 5b, BLT humanized mice were challenged with 20,000 TCID₅₀ HIV_{JRC5F} via intraperitoneal injection. At 48 h after challenge, mice received the HIV-resistant (C34-CXCR4⁺) Dual-CAR TCP consisting of 2×10^7 total CAR T cells. In 1-week intervals after challenge, mice were euthanized and tissues were collected at necropsy. Splenocytes were prepared and freshly sorted; isolated cells were used to quantify the amount of cell-associated HIV DNA harbored within C34-CXCR4⁺ and C34-CXCR4⁻ CAR T cells.

HIV suppression assay. At 7 d following initial activation with anti-CD3/CD28 Dynabeads, we infected primary CD4⁺ T cells with CCR5-tropic HIV_{JRC5F} at a multiplicity of infection (MOI) of 1. After 1 d, we washed HIV-challenged CD4⁺ T cells with complete RPMI supplemented with 100 U ml⁻¹ IL-2 and mixed with CAR. ζ or control untransduced (UTD) T cells at effector-to-target (E/T) ratios of 1:1.25, 1:25, 1:50, 1:100 and 1:200. The E/T ratios reflect the number of CAR. ζ T cells to HIV-challenged, CD4⁺ T cells. Mixtures of cells were plated in triplicate

and HIV replication was measured by sampling 100 μ l per well for flow cytometric detection and intracellular cytokine staining for HIV-1 Core Antigen at 2, 4 and 6 d postcoculture. We added fresh media to each well following staining.

HIV-infected cell elimination assay. A similar target cell elimination assay was performed as described⁶⁹. Here we prepared HIV-infected CD4⁺ T cells as described above. Once 30% of total cells stained positively for HIV-1 Core Antigen, cells were membrane labeled using CellTrace Violet (CTV) (ThermoFisher) to identify HIV-infected cells from CAR or UTD T cells. For characterizing the cytotoxic function of the preinfusion TCP, CAR- ζ and UTD T cells were cultured with CTV-labeled HIV-infected cells at 0.25:1, 1:1 and 4:1 E/T ratios. For ex vivo stimulation, single-cell suspensions of bone marrow from HIV-infected mice treated with the Dual-CAR TCP were cultured with CTV-labeled HIV-infected target cells at 1:1, 5:1 and 10:1 E/T ratios. HIV-infected cells were assessed for the induction of active caspase-3 24 h later by flow cytometry. Active caspase-3 was identified in living CTV⁺ HIV_{GAG}⁺ T cells. The gating strategy is outlined in Supplementary Fig. 1f.

Cytotoxicity, CD107a degranulation and cytokine assays. In vitro CAR T cell functionality was assessed following stimulation of 2×10^5 CAR- ζ or UTD T cells with 2×10^5 K.WT or K562 cells engineered to express the extracellular and transmembrane regions of HIV_{TU2}GP160 (K.Env). Anti-CD107a antibody was included at the beginning of the stimulation followed by 1X Brefeldin A and Monensin Solution (BioLegend) an hour later. In total, cells were incubated for 6 h at 37°C. Cytokine production was measured by flow cytometry and intracellular staining with anti-human antibodies specific for IL-2, IFN- γ , MIP-1 β , TNF and GM-CSF, while cytotoxic potential was measured by staining with antibodies specific for granzyme B and perforin. Cytokine-positive CAR T cells were reported as the difference in the production of cytokines after stimulation with K.Env and K.WT cells.

Measurement of CAR T cell responses ex vivo. Functionality of CAR T cells from HIV-infected BLT humanized mice was measured after ex vivo stimulation with K562 target cells. Density gradient centrifugation was used to isolate mononuclear cells after preparing a single-cell suspension from tissues. Between 0.5 and 1×10^6 mononuclear cells were cultured with 2×10^5 K562.WT or K562.Env cells. The assessment of cytotoxic potential, degranulation and cytokine production was performed using the same protocol described above.

Cell-associated HIV DNA quantitation. Mononuclear cell suspensions obtained from spleens were stained and sorted as described above. After sorting, samples were frozen as cell pellets and stored at -80°C. To obtain genomic DNA, cell pellets were thawed and total DNA was extracted using the QIAamp DNA Mini Kit (QIAGEN) per the manufacturer's protocol. Total HIV DNA was measured in each sample using a multiplexed ddPCR assay specific for HIV *gag* and the human *RPP30* gene. *Gag* forward and reverse amplification primer sequences were 5'-AGTGGGGGACATCAAGCAGCCATGCAAAT and 5'-TGCTATGTCAGTCCCCCTGGTCTCT, respectively. *Gag* sequence was detected using a 5' HEX-labeled hydrolysis probe (HEX-CCATCAATGAGGAAGCTGCAGAAATGGGA). *RPP30* forward and reverse amplification primer sequences were 5'-GATTGGACCTGCGAGCG and 5'-GCGGCTGTCTCCACAAGT, respectively. Human *RPP30* sequence was detected with a 5' 6-FAM-labeled hydrolysis probe (6-FAM-CTGACCTGAAGGCTCT). The *RPP30* primer/probe set has been described previously⁷⁰. ddPCR reactions were performed using the manufacturer-recommended consumables and the ddPCR supermix for probes (No UTP) (Bio-Rad). Thermal cycling conditions are as follows: 1 cycle of 95°C for 10 min, 45 cycles of 94°C for 30 s followed by 60°C for 1 min, 1 cycle of 98°C for 10 min. Droplets were generated using a QX100 droplet generator and subsequently analyzed on a QX200 droplet reader (Bio-Rad) using the QuantaSoft v.1.7.4.0917 software (Bio-Rad). All samples were run in duplicate.

vRC assay. In vitro replication assays were performed essentially as previously described⁵⁷. Human PBMCs were isolated from whole blood by density gradient centrifugation using Histopaque-1077 (Sigma). PBMCs were stimulated with 3 μ g ml⁻¹ phytohemagglutinin (PHA) in complete RPMI (1% Penicillin-Streptomycin, 2 mM L-Glutamine, 25 mM HEPES buffer and 10% FCS) supplemented with 20 U ml⁻¹ recombinant human IL-2 at a concentration of 1×10^6 cells ml⁻¹. After 72 h of stimulation, PBMCs were washed twice with complete RPMI, and resuspended in complete RPMI supplemented with 50 U ml⁻¹ IL-2 at a concentration of 5×10^6 cells ml⁻¹. Cells were infected by spinoculation at 1,200 r.p.m. and 25°C for 2 h. Cells were then washed five times to remove excess virus, and plated in 500 μ l of complete RPMI including 50 U ml⁻¹ IL-2 in a 48-well plate. Infections were incubated at 37°C and 5% CO₂, and 50 μ l of media was removed every 2 d and frozen. Supernatant Gag p24 levels were measured using the Alliance HIV-1 p24 antigen ELISA kit per the manufacturer's instructions (PerkinElmer). Plates were read on a Tecan Infinite 200 Pro plate reader (Tecan Life Sciences) using the Magellan software v.7.2. All infections were carried out in triplicate.

Statistical analysis. Statistical analyses were performed using JMP Pro v.14.2.0 (SAS Institute) and Prism v.7 for PC v.7.05 and Prism v.8 for macOS v.8.2.1 (GraphPad). Spearman rank correlation was used to test for all bivariate continuous correlations. Wilcoxon rank-sum test was conducted to test for all one-way comparisons of means from unpaired samples, and Wilcoxon matched-pairs signed rank test was used for comparing means of paired samples. Kaplan–Meier survival curves were performed using an endpoint defined as the limit of detection of the viral load quantification assay (1.81 log RNA copies per ml), and statistics are generated from the log-rank test. *K*-means clustering was performed using the JMP Pro v.12 statistical package to generate principal component plots with circles denoting where 90% of the observations would fall. We performed area-under-the-curve calculations in GraphPad Prism v.7 using cell concentration data normalized to 1 µl of blood. Additional information regarding how sample sizes were determined and randomized for mouse experiments can be found in the Nature Research Reporting Summary.

Reporting Summary. Further information on research design is available in the Nature Research Reporting Summary linked to this article.

Data availability

All of the construct sequences described in this article are published (see ref. ²⁶). All materials described in this manuscript are available via a material transfer agreement with the University of Pennsylvania or the Ragon Institute. All data are available from the corresponding authors upon request. Source data are provided with this paper.

References

61. Dudek, T. E. et al. Rapid evolution of HIV-1 to functional CD8⁺ T cell responses in humanized BLT mice. *Sci. Transl. Med.* **4**, 143ra198 (2012).
62. Claiborne, D. T. et al. Immunization of BLT humanized mice redirects T cell responses to Gag and reduces acute HIV-1 viremia. *J. Virol.* **93**, e00814–e00819 (2019).
63. Pardi, N. et al. Administration of nucleoside-modified mRNA encoding broadly neutralizing antibody protects humanized mice from HIV-1 challenge. *Nat. Commun.* **8**, 14630 (2017).
64. Boutwell, C. L., Rowley, C. F. & Essex, M. Reduced viral replication capacity of human immunodeficiency virus type 1 subtype C caused by cytotoxic-T-lymphocyte escape mutations in HLA-B57 epitopes of capsid protein. *J. Virol.* **83**, 2460–2468 (2009).
65. Johnson, D. et al. Expression and structure of the human NGF receptor. *Cell* **47**, 545–554 (1986).
66. Wang, X. et al. A transgene-encoded cell surface polypeptide for selection, in vivo tracking, and ablation of engineered cells. *Blood* **118**, 1255–1263 (2011).
67. Brelot, A., Heveker, N., Montes, M. & Alizon, M. Identification of residues of CXCR4 critical for human immunodeficiency virus coreceptor and chemokine receptor activities. *J. Biol. Chem.* **275**, 23736–23744 (2000).
68. Richardson, M. W. et al. Mode of transmission affects the sensitivity of human immunodeficiency virus type 1 to restriction by rhesus TRIM5α. *J. Virol.* **82**, 11117–11128 (2008).
69. Clayton, K. L. et al. Resistance of HIV-infected macrophages to CD8⁺ T lymphocyte-mediated killing drives activation of the immune system. *Nat. Immunol.* **19**, 475–486 (2018).
70. Hindson, B. J. et al. High-throughput droplet digital PCR system for absolute quantitation of DNA copy number. *Anal. Chem.* **83**, 8604–8610 (2011).

Acknowledgements

We thank C. Ellebrecht and A. Payne (University of Pennsylvania) for the HIV_{v12} Envelope-transduced K562 cell line. We thank W. Garcia-Beltran for artistic contributions. This study was supported by NIH grants P01HL129903 (T.M.A.), U19AI117950 (J.L.R.) and UM1AI126620 (J.L.R.) funded by NIAID, NIDA, NIMH and NINDS; T32 grant AI007632 (C.R.M.); and an NIAID F32 grant AI136750 (D.T.C.). We also acknowledge support from the Ragon Institute of MGH, MIT and Harvard and the MGH Scholars program (T.M.A.). We thank the Human Immune System Mouse Core at the Ragon Institute of MGH, MIT and Harvard and the Stem Cell and Xenograft Core at the University of Pennsylvania for the generation of BLT humanized mice, the Penn Center for AIDS Research (P30-AI045008) for purified human T cells, and the Allen and Riley laboratories for helpful comments.

Author contributions

C.R.M., D.T.C., K.O., C.L.B., J.L.R. and T.M.A. conceived and designed the project and contributed to the interpretation of data. C.R.M., D.T.C., K.O., T.C., D.L.D., X.S., K.A.P., R.T.T., K.K., M.P., V.D.V., S.T., T.B., G.J.L. and J.A.H. contributed to the acquisition and analysis of data. C.R.M., D.T.C., C.L.B., J.L.R. and T.M.A. drafted the manuscript.

Competing interests

C.R.M. and J.L.R. have filed an institution-owned patent (20180265565: Method of Redirecting T Cells to Treat HIV Infection) describing the construction of these HIV-specific CARs specific to Figs. 1 and 2. This patent application has been published but has not yet been granted. C.R.M. and J.L.R. have also filed an institution-owned patent (Dual CAR Expressing T Cells Individually Linked to CD28 and 4-1BB) specific to Figs. 4–6. G.J.L., J.A.H. and J.L.R. have also filed an institution-owned patent (Non-Signaling HIV Fusion Inhibitors And Methods Of Use Thereof) specific to Figs. 5 and 6. J.L.R. cofounded a company called Tmunity Therapeutics that has the rights to license the technology described in this paper. J.L.R. holds an equity interest in Tmunity. C.R.M. and J.L.R. declare no other competing financial interests. No other authors declare any competing financial interests. No authors declare any nonfinancial interests.

Additional information

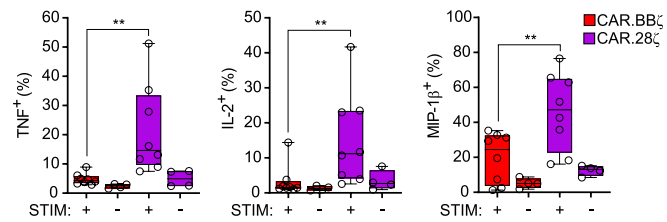
Extended data is available for this paper at <https://doi.org/10.1038/s41591-020-1039-5>.

Supplementary information is available for this paper at <https://doi.org/10.1038/s41591-020-1039-5>.

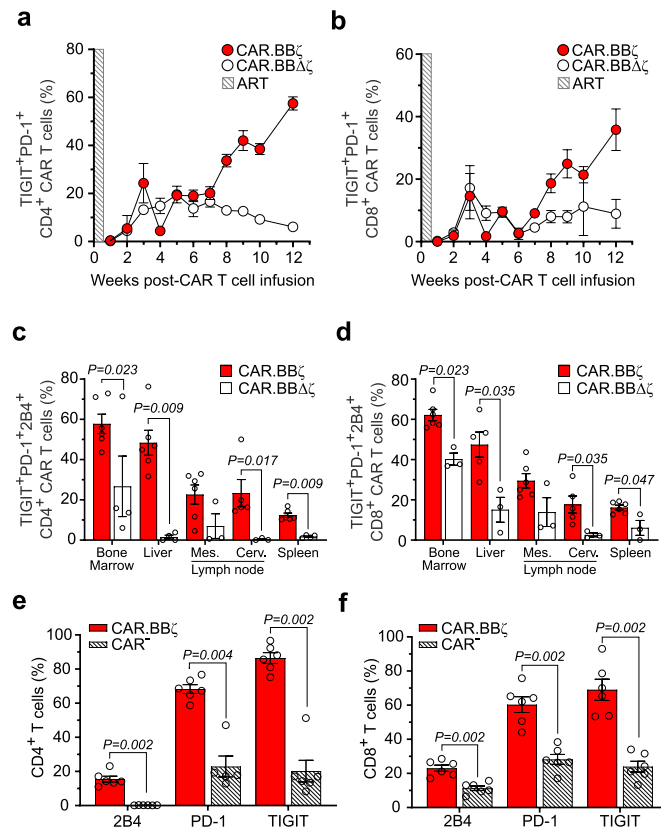
Correspondence and requests for materials should be addressed to J.L.R. or T.M.A.

Peer review information Alison Farrell was the primary editor on this article and managed its editorial process and peer review in collaboration with the rest of the editorial team.

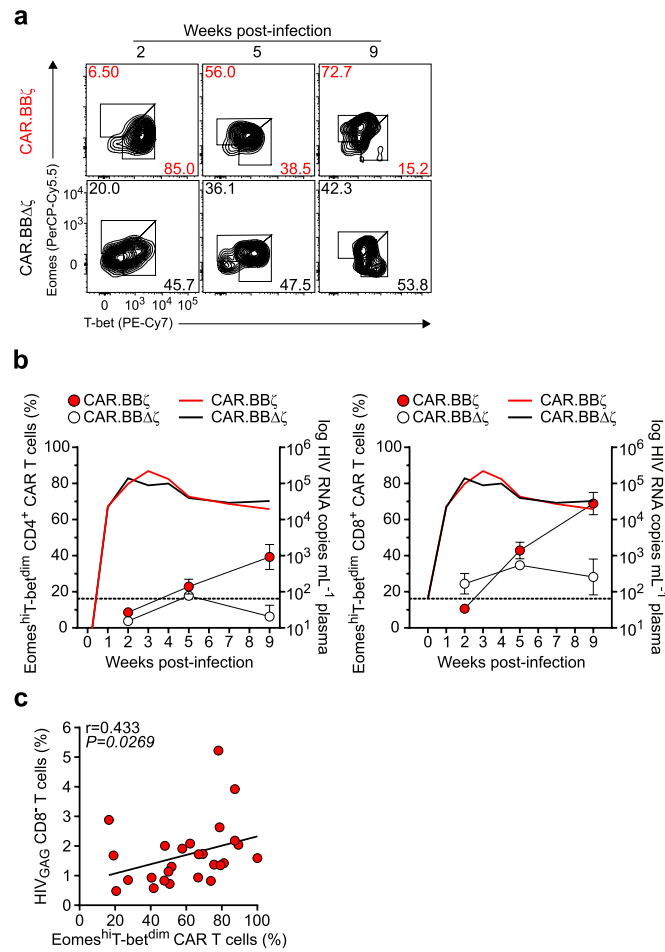
Reprints and permissions information is available at www.nature.com/reprints.



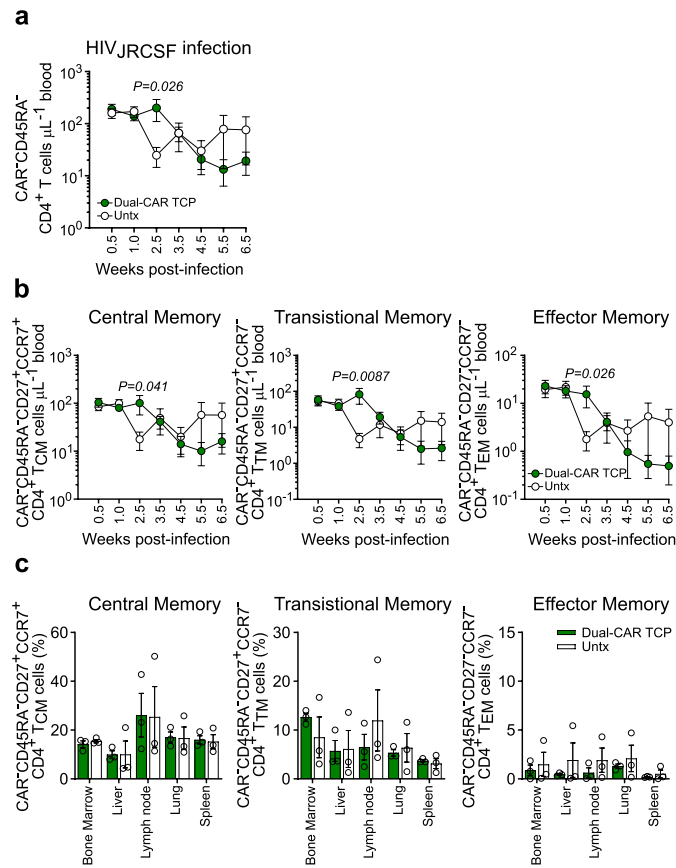
Extended Data Fig. 1 | CD28 costimulation enhances the ex vivo effector function of CAR T cells. HIV-uninfected mice were infused with an equal mixture of CD4-based CAR T cells expressing either CD3-ζ, 4-1BB/CD3-ζ and CD28/CD3-ζ costimulatory domains linked to unique fluorescent proteins to facilitate identification in vivo as described in Fig. 2 legend. Cumulative data indicating the frequency of TNF⁺, IL-2⁺ and MIP-1β⁺ CAR.BBζ and CAR.28ζ T cells within the same mice after ex vivo stimulation with K.Env (+) or K.WT (-) cells. Data represents the aggregate of cytokine producing cells from liver and terminal blood (n = 8). CAR.ζ T cells were too infrequent for analysis. Data shows box and whisker plots where the middle line indicates median, bounds of the box show 25th to 75th percentiles, and bars extend to min and max values. Symbols represent biologically independent animals. Significance was calculated using two-sided Wilcoxon matched-pairs signed rank test.



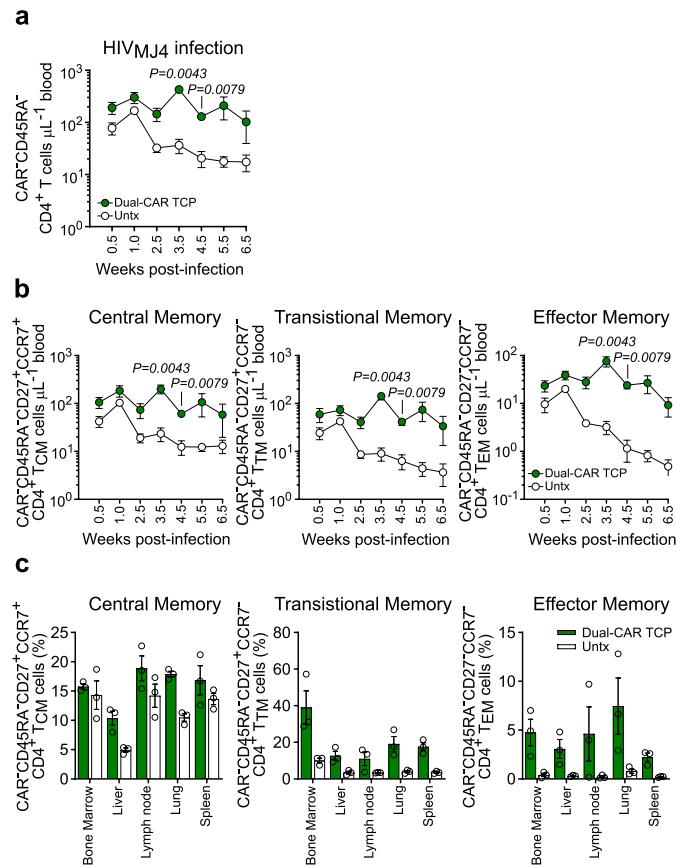
Extended Data Fig. 2 | CAR.BB ζ T cells accumulate multiple inhibitory receptors as disease progresses. **a**, Frequency of CD4⁺ and **(b)** CD8⁺ CAR.BB ζ T cells (G1; n=6) and CAR.BB $\Delta\zeta$ T cells (G2; n=6) co-expressing TIGIT and PD-1 after infusion. Shaded box indicates the window of ART. Symbols and error bars indicate mean \pm SEM. **c**, Frequency of CD4⁺ and **(d)** CD8⁺ CAR.BB ζ T cells (G1) and CAR.BB $\Delta\zeta$ T cells (G2) co-expressing TIGIT, PD-1 and 2B4 in tissues 12 weeks post-infusion. **e**, Cumulative data indicating the frequency of 2B4⁺, PD-1⁺ and TIGIT⁺ CD4⁺ CAR.BB ζ T cells (G1) compared to CAR⁻ CD4⁺ T cells (G1) within the spleens of the same mice, and **(f)** CD8⁺ CAR.BB ζ T cells (G1) compared to CAR⁻ CD8⁺ T cells (G1) within the spleens of the same mice. **c-f**, Bars indicate mean, error bars show \pm SEM and symbols represent individual mice. Significance was calculated using two-sided Wilcoxon rank-sum test. Sample sizes in these studies represent biologically independent animals.



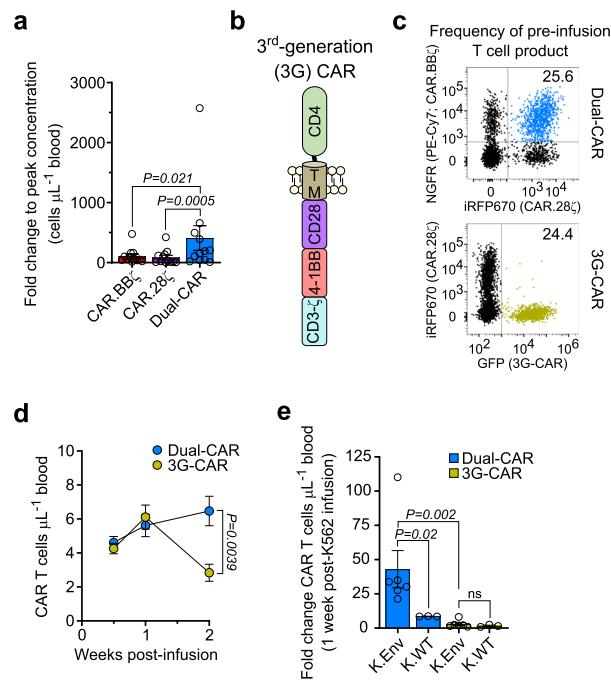
Extended Data Fig. 3 | Eomes^{hi}T-bet^{dim} CAR.BB ζ T cells accumulate from acute to chronic phases of infection. BLT mice were infected with HIV_{JRC5F} and infused 48 h later with either 2×10^7 CAR.BB ζ T cells ($n=5$) or inactive control CAR.BB $\Delta\zeta$ T cells ($n=3$). **a**, FACS plots show the change in Eomes and T-bet expression within the different CAR T cell types over time. **b**, Summary data indicating the longitudinal frequency of Eomes^{hi}T-bet^{dim} CD8⁺ (left panel) and CD4⁺ (right panel) CAR T cells (left y-axis), and mean log plasma HIV RNA (copies mL⁻¹) (right y-axis). Thin dotted line denotes limit of viral load quantification. Symbols and error bars indicate mean \pm SEM. **c**, Spearman correlation analysis of frequency of Eomes^{hi}T-bet^{dim} CD8⁺ CAR.BB ζ T cells compared with viral burden measured as the frequency of HIV_{GAG}⁺ CD8⁻ T cells in various tissues 10 weeks post-infection. Sample sizes in these studies indicate biologically independent animals.



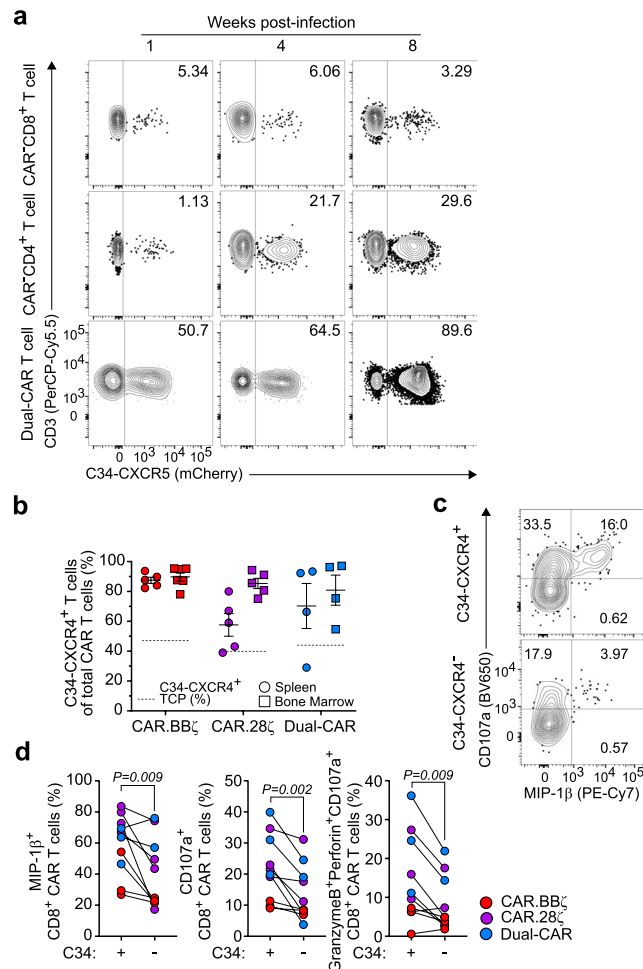
Extended Data Fig. 4 | Dual-CAR T cell product transiently delays CD4⁺ T cell loss despite persistent HIV_{JRCSF} infection. BLT mice received Dual-CAR T cell product (TCP) (n = 6) 48 h after HIV_{JRCSF} challenge, while control mice were untreated (Untx) (n = 5). **a**, Concentration of peripheral total memory CD4⁺ T cells (CAR⁻). **b**, Concentration of peripheral central memory (CD45RA⁻CD27⁺CCR7⁺; left panel), transitional memory (CD45RA⁻CD27⁺CCR7⁻; middle panel), and effector memory (CD45RA⁻CD27⁻CCR7⁻; right panel) CD4⁺ T cells (CAR⁻). **c**, Frequency of memory CD4⁺ T cell (CAR⁻) subsets in tissues 8 weeks post-infection. **a**, **b**, Significance was calculated using a two-sided Wilcoxon rank-sum test. Symbols and bars indicate mean, and error bars show \pm SEM. Sample sizes indicate biologically independent animals.



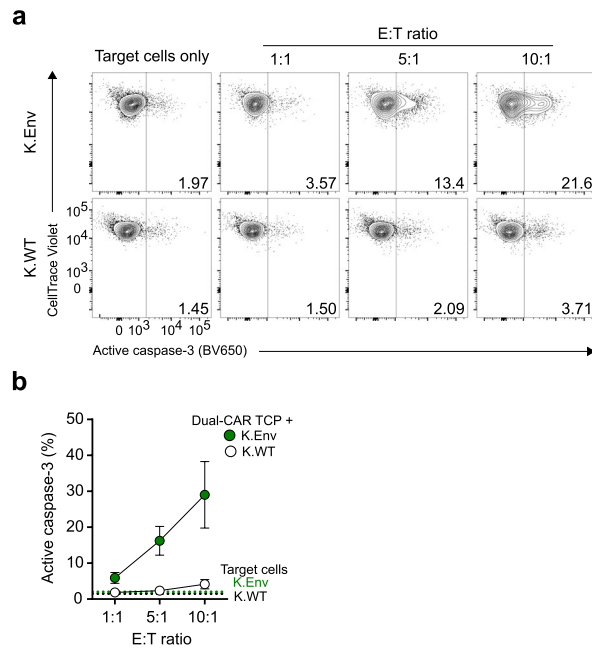
Extended Data Fig. 5 | Dual-CAR T cell product prevents CD4⁺ T cell loss despite persistent HIV_{M14} infection. BLT mice were infused with Dual-CAR T cell product (TCP) ($n=6$) 48 h post-HIV_{M14} challenge, while control mice were untreated (Untx) ($n=6$). **a**, Concentration of peripheral total memory CD4⁺ T cells (CAR⁺). **b**, Concentration of peripheral central memory (CD45RA⁻CD27⁺CCR7⁺; right panel), transitional memory (CD45RA⁻CD27⁺CCR7⁻; middle panel), and effector memory (CD45RA⁻CD27⁻CCR7⁻; left panel) CD4⁺ T cells (CAR⁺). **c**, Frequency of memory CD4⁺ T cell (CAR⁺) subsets in tissues 8 weeks post-infection. **a**, **b**, Significance was calculated using a two-sided Wilcoxon rank-sum test. Symbols and bars indicate mean, while error bars show \pm SEM. Sample sizes indicate biologically independent animals.



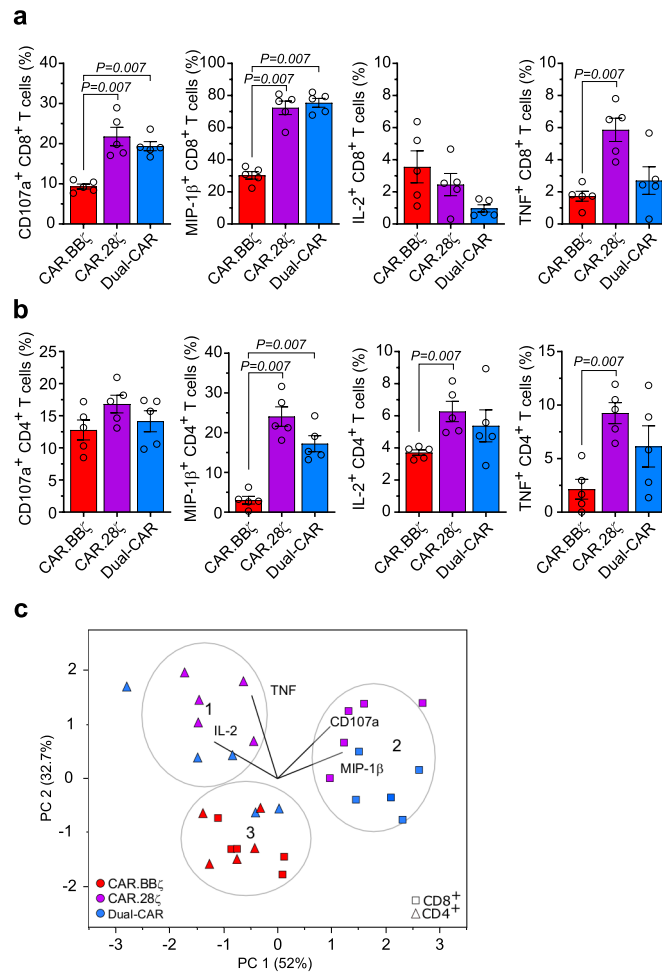
Extended Data Fig. 6 | Dual-CAR T cells exhibit superior in vivo expansion compared to 4-1BB-costimulated, CD28-costimulated, and 3rd-generation CAR T cells. **a**, BLT mice were challenged with either HIV_{JRC5F} ($n=6$) or HIV_{M14} ($n=6$) and infused with 2×10^7 Dual-CAR T cell product (TCP). Fold-change in CAR T cell concentration from baseline to peak levels in peripheral blood. Data is the aggregate of both infection cohorts. **b**, Schematic shows the structural components of the 3rd-generation (3G) CD4-based CAR construct. **c–e**, Dual-CAR T cell product and 3G-CAR T cells were combined at an equal frequency prior to infusion into uninfected mice ($n=9$). **c**, FACS plots indicate the frequency of Dual-CAR and 3G-CAR T cells present within the pre-infusion T cell product. **d**, Longitudinal concentration of peripheral CAR T cells following adoptive transfer into HIV-negative mice. Symbols and error bars indicate mean \pm SEM. **e**, At 2 weeks post-infusion, mice received either 10^7 irradiated K.Env cells ($n=6$) or 10^7 irradiated K.WT cells ($n=3$). Fold change in the concentration of peripheral CAR T cells 1-week post-K562 infusion from baseline concentration prior to K562 infusion. **a**, **d**, **e**, Bar and error bars indicate mean \pm SEM, and symbols represent individual mice. **a**, **d**, **e**, Two-sided Wilcoxon rank-sum test was used to calculate significance. Sample sizes in these studies indicate biologically independent animals.



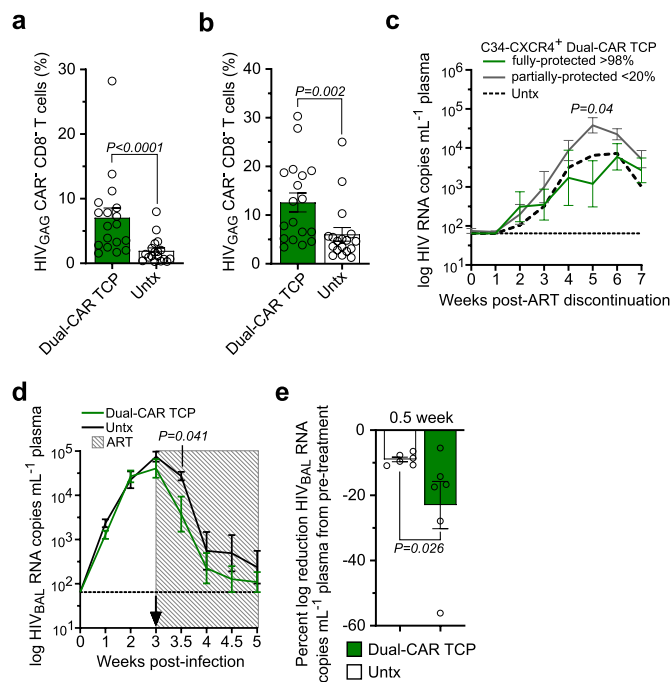
Extended Data Fig. 7 | C34-CXCR4⁺ CAR T cells are selected for during chronic infection and exhibit superior ex vivo effector functions. **a**, BLT mice were infected with HIV_{IRCSF} and 48 h later infused with 10⁷ C34-CXCR4⁺ Dual-CAR T cell product (TCP). FACS plots indicate the frequency of C34-CXCR4⁺ throughout infection. **b**, Mice were infected with HIV_{MJ4} and 48 h later were infused with 10⁶ C34-CXCR4⁺ CAR.BBζ (n=5), CAR.28ζ (n=5), or purified Dual-CAR (n=4) T cells. Frequency of C34-CXCR4⁺ CAR T cells in tissue 8 weeks post-infection. Thin dotted line indicates the frequency of C34-CXCR4⁺ CAR T cells in the pre-infusion TCP for the indicated CAR T cell type. Line and error bars indicate mean ± SEM. **c**, **d**, Mice were infected with HIV_{MJ4} and 48 h later received 10⁶ C34-CXCR4⁺, purified CAR.BBζ.BBζ (n=3), CAR.28ζ.28ζ (n=4), or Dual-CAR (n=3) T cells. **c**, FACS plots and **(d)** cumulative data show the frequency of each CD8⁺ CAR T cell population expressing MIP-1β and CD107a, and the frequency of CAR T cells with cytotoxic potential (granzyme B⁺ perforin⁺ CD107a⁺). CAR T cells were isolated from the spleen and bone marrow of mice 8 weeks post-infection and ex vivo stimulated. Significance was calculated using two-sided Wilcoxon matched-pairs signed rank test. For all data, symbols represent individual mice. Sample sizes in these studies indicate biologically independent animals.



Extended Data Fig. 8 | CAR T cells from HIV-infected mice exhibit ex vivo cytotoxic function. HIV_{JRCSF}-infected mice (n = 3) treated with the Dual-CAR TCP were euthanized and the bone marrow cells were ex vivo stimulated with K.Env or K.WT cells for 24 h at the indicated E:T ratios. **a**, Representative FACS plots and **(b)** cumulative data shows the induction of active caspase-3 within the different target cell populations. Symbols and error bars indicate mean ± SEM. Sample size indicates biologically independent animals.



Extended Data Fig. 9 | Dual-CAR and CAR.28 ζ T cells exhibit similar ex vivo functional profiles. BLT mice were challenged with HIV_{JRCSF} (n=5) and infused with 2×10^7 Dual-CAR T cell product (TCP) 48-hours post infection. **a**, Frequency of CD8⁺ and **(b)** CD4⁺ CAR T cell populations from tissue at necropsy (8-weeks post-infection) within the same mice expressing CD107a, MIP-1 β , IL-2 and TNF after ex vivo stimulation. Bars and error bars indicate mean \pm SEM, and symbols represent individual mice. Significance was calculated using two-sided Wilcoxon rank-sum test. **c**, Principle Components Analysis (PCA) of IL-2, TNF, MIP-1 β , and CD107a expression in ex vivo stimulated CD8⁺ and CD4⁺ CAR T cells from PBMCs of HIV_{JRCSF}-infected mice (n=5). Sample sizes in these studies represent biologically independent animals.



Extended Data Fig. 10 | HIV-resistant Dual-CAR TCP reduces virus replication in vivo. **a**, Frequency of HIV_{GAG}⁺ CD8⁺ T cells (CAR⁺) within the bone marrow and spleen of HIV_{JRC5F}-infected mice (n = 6) and **(b)** HIV_{MJ4}-infected mice (n = 6) that were treated 48 h post-challenge with the Dual-CAR T cell product (TCP) or were untreated (Untx). **c**, Mean log plasma HIV_{MJ4} RNA (copies mL⁻¹) after ART discontinuation of mice infused at ART initiation with 10⁷ protected >98% C34-CXCR4⁺ (n = 5) or partially-protected <20% C34-CXCR4⁺ (n = 7) Dual-CAR TCP, or were untreated (n = 9). **d**, **e**, HIV_{BAL}-infected mice were ART-treated and simultaneously infused with 10⁷ HIV-resistant Dual-CAR TCP (n = 6) or were untreated (n = 6). **d**, Mean log plasma HIV RNA (copies mL⁻¹). Shaded box indicates ART and arrow indicates CAR TCP infusion. **e**, Percent log reduction in plasma HIV RNA from pre-ART (week 3) and 0.5 and 1 week post-ART. For all data, bars and error bars indicate mean ± SEM, and symbols represent individual mice. Significance was calculated for **(a-d)** by two-sided Wilcoxon rank-sum test and **(e)** two-sided Kolmogorov-Smirnov test. Sample sizes in these studies indicate biologically independent animals.

Reporting Summary

Nature Research wishes to improve the reproducibility of the work that we publish. This form provides structure for consistency and transparency in reporting. For further information on Nature Research policies, see [Authors & Referees](#) and the [Editorial Policy Checklist](#).

Statistics

For all statistical analyses, confirm that the following items are present in the figure legend, table legend, main text, or Methods section.

n/a Confirmed

- The exact sample size (n) for each experimental group/condition, given as a discrete number and unit of measurement
- A statement on whether measurements were taken from distinct samples or whether the same sample was measured repeatedly
- The statistical test(s) used AND whether they are one- or two-sided
Only common tests should be described solely by name; describe more complex techniques in the Methods section.
- A description of all covariates tested
- A description of any assumptions or corrections, such as tests of normality and adjustment for multiple comparisons
- A full description of the statistical parameters including central tendency (e.g. means) or other basic estimates (e.g. regression coefficient) AND variation (e.g. standard deviation) or associated estimates of uncertainty (e.g. confidence intervals)
- For null hypothesis testing, the test statistic (e.g. F , t , r) with confidence intervals, effect sizes, degrees of freedom and P value noted
Give P values as exact values whenever suitable.
- For Bayesian analysis, information on the choice of priors and Markov chain Monte Carlo settings
- For hierarchical and complex designs, identification of the appropriate level for tests and full reporting of outcomes
- Estimates of effect sizes (e.g. Cohen's d , Pearson's r), indicating how they were calculated

Our web collection on [statistics for biologists](#) contains articles on many of the points above.

Software and code

Policy information about [availability of computer code](#)

Data collection

BD FACSDiva Software version 8.0.1 (Flow cytometry)
QuantaSoft version 1.7.4.0917 (ddPCR)
LightCycler 480 Software release 1.5.1.62 SP3 (real-time PCR)
Viia 7 QuantStudio Real-time PCR Software v1.3 (real-time PCR)
Magellan version 7.2 (Tecan plate reader)

Data analysis

Prism 8 for macOS version 8.2.1
Prism 7 for PC version 7.05
JMP Pro version 14.2.0
Flowjo software version 10

For manuscripts utilizing custom algorithms or software that are central to the research but not yet described in published literature, software must be made available to editors/reviewers. We strongly encourage code deposition in a community repository (e.g. GitHub). See the Nature Research [guidelines for submitting code & software](#) for further information.

Data

Policy information about [availability of data](#)

All manuscripts must include a [data availability statement](#). This statement should provide the following information, where applicable:

- Accession codes, unique identifiers, or web links for publicly available datasets
- A list of figures that have associated raw data
- A description of any restrictions on data availability

All of the construct sequences described in this article are published (see Leibman et al. PMID 29023549). All materials described in this manuscript are available via a material transfer agreement with the University of Pennsylvania or the Ragon Institute. All data are available from the corresponding authors upon request.

Field-specific reporting

Please select the one below that is the best fit for your research. If you are not sure, read the appropriate sections before making your selection.

Life sciences Behavioural & social sciences Ecological, evolutionary & environmental sciences

For a reference copy of the document with all sections, see [nature.com/documents/nr-reporting-summary-flat.pdf](https://www.nature.com/documents/nr-reporting-summary-flat.pdf)

Life sciences study design

All studies must disclose on these points even when the disclosure is negative.

Sample size	In general, study arms were designed with sample sizes of 8 mice per group in order to provide an adequate power (80% or more) to detect an effect size of 1.60. These power calculations were based on simulation studies using 10,000 Monte Carlo samples and two-sided Wilcoxon rank sum test with type 1 error rate of 5%. However, due to the nature of the model system used (BLT humanized mice), batch sizes are variable as they are determined by the quality and size of the human donor tissue. As such, sample sizes were chosen to balance statistical power with the need to test treatment arms within the same donor batch of BLT mice. For example, when sample sizes were small due to batch size restrictions, non-parametric statistical tests were used. In general, sample sizes of no less than 6 mice were used in a given study. Animal studies in which experimental arms fell below the target of 8 mice were repeated in independent experiments to confirm findings.
Data exclusions	No data points were excluded from the analyses detailed in this manuscript.
Replication	In essence, all major findings were replicated in multiple batches of BLT humanized mice, and all attempts at replication were successful. For example: 1) Non-inferiority of BLT-derived CAR T cells. In vitro experiments comparing CAR T cell functions in BLT T cell-derived and human PB-derived CAR T cells were performed using 3 distinct BLT mouse samples representing 3 genetically distinct donor sources as well as 3 distinct adult human PMBC donors (Fig. 1 and Fig. S1). 2) Costimulatory domain effects. Data shown in Fig. 2 regarding effects of 4-1BB vs CD28 costimulation integrated into the CAR, were observed again in Fig. 4 and Fig. 5, representing 4 distinct batches of BLT mice generated from 4 genetically distinct donor tissues. 3) Dual CARs demonstrate superior effector functions in vivo. Controlled studies in which purified populations of 41BBz/CD28z Dual CARs were shown to demonstrate enhanced in vivo expansion and protection from CD4+ T cell loss (Fig. 5c,d, Fig. S16) were repeated in a completely distinct BLT cohort (Fig. 5f,g, Fig. S18), and further controlling for CAR expression levels by purifying doubly transduced 41BBz/41BBz CARs and CD28z/CD28z CARs alongside Duals CARs and by the same manufacturing and selection process (Fig. S17). 4) HIV-susceptible CAR T cells increase acute viremia and/or HIV rebound. Data demonstrating this finding and depicted in Fig. 6a are derived from 6 independent studies. 5) Acceleration of viral control when CAR T cells given at the time of ART initiation. This result was repeated in two distinct batches of BLT mice, generated at two different facilities and with two different HIV isolates, depicted in Fig. 6e,f and Fig. S21d,e.
Randomization	Due to variability in reconstitution levels and phenotypes among humanized mice, groups were normalized rather than randomized in order to limit bias in experimental groups. In general, groups were normalized using data from pre-study blood draws and flow cytometry-based phenotyping on the following criteria: - # of CD4+ T cells/uL of blood - # of CCR5+ CD4+ T cells/uL of blood - % of memory CD4+ T cells - Weight of the mice at study start (health status) - Plasma viral load (where applicable)
Blinding	Technicians responsible for blood and tissue collection were blinded to the study groups. Blood processing and downstream flow cytometry and qRT-PCR for viral loads were performed without strict identification of study groups, only mouse identifiers. Mouse IDs and data were formally assigned to study groups only at the time of data analysis.

Reporting for specific materials, systems and methods

We require information from authors about some types of materials, experimental systems and methods used in many studies. Here, indicate whether each material, system or method listed is relevant to your study. If you are not sure if a list item applies to your research, read the appropriate section before selecting a response.

Materials & experimental systems

n/a	Involved in the study
<input type="checkbox"/>	<input checked="" type="checkbox"/> Antibodies
<input type="checkbox"/>	<input checked="" type="checkbox"/> Eukaryotic cell lines
<input checked="" type="checkbox"/>	<input type="checkbox"/> Palaeontology
<input type="checkbox"/>	<input checked="" type="checkbox"/> Animals and other organisms
<input type="checkbox"/>	<input checked="" type="checkbox"/> Human research participants
<input checked="" type="checkbox"/>	<input type="checkbox"/> Clinical data

Methods

n/a	Involved in the study
<input checked="" type="checkbox"/>	<input type="checkbox"/> ChIP-seq
<input type="checkbox"/>	<input checked="" type="checkbox"/> Flow cytometry
<input checked="" type="checkbox"/>	<input type="checkbox"/> MRI-based neuroimaging

Antibodies

Antibodies used	<p>Format: antigen specificity (clone; cat#)</p> <p>BioLegend: CD45 (HI30 and 2D1; 304023 and 368513), CD19 (HIB19; 302251), CD3 (OKT3; 317335), CD4 (OKT4 and RPA-T4; 317415 and 300553), CD8 (RPA-T8 and SK1; 301065 and 344745), CD45RA (HI100; 304125 and 304110), CD27 (LG.3A10; 124229), CCR7 (G043H7; 353211), CCR5 (J418F1; 359107), CD271 (ME20.4; 345107 and 345109), PD-1 (EH12.2H7; 329919), TIGIT (VSTM3; 372715), 2B4 (C1.7; 329521), CD107a (H4A3; 328637), IL-2 (MQH-17H12; 500331), Perforin (B-D48; 353303 and 353307), anti-mouse CD45 (30-F11; 103115), CD20 (2H7; 302313), CD14 (HCD14; 325619), CD56 (HCD56; 318331)</p> <p>BD Biosciences: CD45 (HI30; 564106), CD3 (UCHT1; 612941), CD8 (SK1; 612889), CD45RA (HI100; 612846), CCR7 (3D12; 560922), TNF (Mab11; 563996), IFN-γ (4S.B3; 612845), Granzyme B (GB11; 563389), MIP-1β (D21-1351; 560687), GM-CSF (BVD2-21C11; 562857), Active Caspase-3 (C92605; 564096)</p> <p>R&D: Human EGFR (Cetuximab Biosimilar, Hu1; FAB9577G-100)</p> <p>Beckman Coulter: HIV-1 Core Antigen (KC57; 6604667)</p> <p>eBioscience: T-bet (4B10; 25-5825-80), EOMES (WD1928; 46-4877-42), TOX (TXRX10; 12-6502-82)</p>
Validation	<p>Antibody validation was performed by the manufacturer for all antibodies listed.</p> <p>Before use, all antibodies were validated and titrated on human peripheral blood mononuclear cells and the optimal dilution was found to be 1:100.</p> <p>Antibodies used to detect production of effector cytokines (IL-2, TNF, GM-CSF, INF-gamma, and MIP-1B) were validated and titrated on PMA/Ionomycin-stimulated human PBMCs and optimal staining dilutions were found to be between 1:50 to 1:400 for all antibodies tested.</p>

Eukaryotic cell lines

Policy information about [cell lines](#)

Cell line source(s)	<p>HEK 293T/17 cells - ATCC</p> <p>K562 (wild type) – ATCC</p> <p>K562.Env - C. Ellebrecht and A. Payne, University of Pennsylvania</p>
Authentication	<p>ATCC uses morphology, karyotyping, and PCR based approaches to confirm the identity of human cell lines and to rule out both intra- and interspecies contamination. These include an assay to detect species specific variants of the cytochrome C oxidase I gene (COI analysis) to rule out inter-species contamination and short tandem repeat (STR) profiling to distinguish between individual human cell lines and rule out intra-species contamination.</p>
Mycoplasma contamination	<p>All cell lines were tested for mycoplasma contamination using the Lonza MycoAlert assay and were found to be negative.</p>
Commonly misidentified lines (See ICLAC register)	<p>No commonly misidentified cell lines were used in this study.</p>

Animals and other organisms

Policy information about [studies involving animals](#); [ARRIVE guidelines](#) recommended for reporting animal research

Laboratory animals	<p>Mus musculus; NOD.Cg-Prkdcscid Il2rgtm1Wjl/SzJ (NSG); female or male; 6-8 weeks of age at time of humanization; 18-24 weeks of age at time of study start</p>
Wild animals	<p>No wild animals were used in this study.</p>
Field-collected samples	<p>No field collected samples were used in this study.</p>
Ethics oversight	<p>Humanized mouse experiments performed at the Ragon Institute of MGH, MIT and Harvard were approved by the Massachusetts General Hospital Institutional Animal Care and Use Committee (IACUC) under the approved protocol 2016N000483. Humanized mouse experiments performed at the University of Pennsylvania were approved by the University of Pennsylvania IACUC under the approved protocol 805606. All animal studies were carried out in accordance with recommendations in the Guide for the Care and Use of Laboratory Animals of the National Institutes of Health.</p>

Note that full information on the approval of the study protocol must also be provided in the manuscript.

Human research participants

Policy information about [studies involving human research participants](#)

Population characteristics	<p>Human fetal tissue was obtained from a third party commercial supplier. The population comprised pregnant females located in California. No other demographic information is available.</p>
Recruitment	<p>Participants had previously decided to have an abortion and had previously completed an informed consent for the abortion prior to being recruited by a third party commercial supplier to donate aborted material for research purposes. No other information about recruitment is available.</p>

Ethics oversight

The use of anonymized fetal tissue purchased from the third party commercial supplier was deemed Not Human Subjects Research by the Partners Healthcare Institutional Review Board.

Note that full information on the approval of the study protocol must also be provided in the manuscript.

Flow Cytometry

Plots

Confirm that:

- The axis labels state the marker and fluorochrome used (e.g. CD4-FITC).
- The axis scales are clearly visible. Include numbers along axes only for bottom left plot of group (a 'group' is an analysis of identical markers).
- All plots are contour plots with outliers or pseudocolor plots.
- A numerical value for number of cells or percentage (with statistics) is provided.

Methodology

Sample preparation

Cells were derived from either whole blood or single cell suspensions from tissues collected from BLT-humanized mice. For analysis of peripheral blood, plasma was removed by low speed centrifugation, cells were resuspended in PBS, and whole blood was stained with antibodies prior to fixation of cells and lysis of RBCs. Single cell suspensions were isolated from tissues by layering dissociated tissue cell suspensions over a density gradient and removing the mononuclear cell layer after centrifugation.

Instrument

BD FACSymphony High Parameter Flow Cytometer

Software

BD FACSDiva Software version 8.0.1 (data collection)
FlowJo version 10.5.3 (data analysis)

Cell population abundance

For NGFR selections to purify C34-CXCR4+ cells (Figure 6), post-selection flow was used to determine purities that were >98%.

Gating strategy

General gating strategies were as follows:
lymphocyte gate, human CD45+ and mouse CD45-, CD3+ and other lineage negative, CAR T cell marker positive (i.e. GFP+, iRFP670+, NGFR+), CD4+ for CD8-CAR and CD4-bright for CD4 CAR

Supplementary Figures added to depict specific gating strategies:

- Gating of target cells in in vitro elimination assays, Supplementary Fig. 1f
- Gating of endogenous memory CD4+ T cells, Supplementary Fig. 3a
- Sorting gates for C34-CXCR4+/- CAR T cells, Supplementary Fig. 22a
- Sorting gates for endogenous central memory CD4+ T cells, Supplementary Fig. 22b

- Tick this box to confirm that a figure exemplifying the gating strategy is provided in the Supplementary Information.